Changes of Direction: Forces on the Human Talus

Steven G. Lautzenheiser

A dissertation

submitted in partial fulfillment of the

requirements for the degree of

Doctor of Philosophy

University of Washington

2019

Reading Committee:

Patricia Ann Kramer, Chair

Adam D. Sylvester

Steven M. Goodreau

Program Authorized to Offer:

Anthropology

University of Washington

Abstract

Changes of Direction: Forces on the Human Talus

Steven G. Lautzenheiser

Chair of the Supervisory Committee:

Patricia Ann Kramer, PhD

Department of Anthropology

This dissertation explores the evolution of the human foot by understand the forces that impact foot morphology. The talus is a prime first suspect to focus this endeavor because it is the only bony connection between the foot and the rest of the body. Three separate studies were designed to examine the ability to utilize palpable landmarks to locate the internal location of the talus, to determine if ground reaction forces (GRFs) are different when an individual changes direction while moving, and to examine how the position the foot is placed influences the GRFs applied to the foot. The presented results indicate that the *in vivo* location of the can be predicted reliably from the location of external markers of the navicular tubercle and both malleoli. Due to their close proximity to the talus, it is unsurprisingly that these three bony landmarks were predictive of the location of the joints. Nonetheless, the degree to which variation in internal position of the joints was predicted by external landmarks is encouraging for future FEA of the talus. Changing direction while walking produces higher side forces that are applied to the human foot. I was

able to illustrate the GRF components required to make a turn differ from those required to move in a straight path in both braking and propulsive phases of stance. Finally, the presented results illustrate that foot placement does influence the forces applied to the foot. In both early and late stance, maximum mediolateral forces are greater in the established foot coordinate system (FCS) than the world coordinate system (WCS). The increase in side forces in the FCS averages between 150-200 N, with some individuals exhibiting increases of greater than 350 N. The direction of the force also changes. In WCS the maximum force is directed toward the centerline, while in FCS it is lateral. Since the GRF magnitude does not change, this increase in side forces is due to decreases in the other two components. In the end, this dissertation illustrated that our understanding of how the foot interacts with the ground is more complex than we typically thought as a result of the common phenomenon of changing direction.

Acknowledgements

It has been a long and rewarding process working on this dissertation. So many people have supported and encouraged me in this attaining this degree. First, I would like to thank my dissertation committee: Patricia Kramer, Adam Sylvester, Steve Goodreau and Sarah Stroup.

Thank you for everyone that was part of my research, either by volunteering to be a research participant or an undergraduate research assistant. Without the donation of your time this dissertation would not have been possible.

I would like to thank the various faculty members across this campus that have been there for me, both within out outside of Anthropology. Thank you to Dr. Donald Grayson for letting me torment your amazing zooarchaeology students and being a great mentor. Thank you to Danny Hoffman and Janelle Taylor for your encouragements and never letting me to self-depreciate myself. Thank you to Andrea Duncan for letting me hide in your office to distract myself from whatever coding problem I was having at the time. Thank you to Ellen Feuerriegel for being a great friend and collaborator over these past years and for being one of my greatest allies. Thank you to Greg Wilson for taking me to the field and galvanizing my love for all things paleontological. Thank you to Adam Sylvester for being a great role model and always pushing me to better scientist. Thank you to Stephen Benirschke and the Debs Chair at UW Orthopaedics and Sports Medicine for often funding me over the past six years.

Thank you to my fellow graduate students for always all the great times laughing, crying, or drinking while playing board games. Thank you to cohort, Sarah Stansfield and Rob Tennyson, for being my partners in crime and helping me survive grandmother theory, DOHaD, reproductive senescence, and survivorship analyses. Thank you to Jeannie Bailey for being the

best academic sibling those first few years, until you had to leave the nest. Thank you to Tiffany Pan for always reminding me to sometimes look at the forest and not just the trees.

A very special acknowledgement to Dr. Patricia Kramer, without who this would not be possible. I can't believe our in-class discussions about fossilized feet and how they vary across time would have started me on this path (ha!). I can't express how much of an honor it has been to be welcomed into the lineage. Thank you so much for always encouraging me and pushing me to be the best I can be. This could not have happened without you and I am forever in your debt.

Thank you to my family, those still here and those who I wish could have seen me finish this process. Mom and Dad, thank you for never giving up on me. While we had our ups and downs, you always supported me. Nan and Pop, while you are not physically here, I know you were with me each step of this process. Thank you for starting my journey of exploration of the natural world.

Finally, I want to thank my partner Bryan. You were always there for be providing unconditional love, support, and unending patience. I know this process was not always easy on you. I'm sorry for the countless hours helping me study muscle originations, practicing lectures, or just being my shoulder to cry on while I vented frustration. I could not ask for a more understanding and patient partner. Without you I could not have made it through these past six years.

Table of Contents

Chapter 1: Introduction

Our knowledge of the evolution of hominin foot forms remains obscure (Harcourt-Smith & Aiello, 2004). In part, this is due to the relative paucity of relevant fossil material. In addition, however, we lack compelling models that connect form and function in the modern foot; models that would then allow us to better understand the meaning of the fragmentary fossil record available to us. The change from a mobile, grasping foot, characteristic of primates, to a more rigid, plantigrade foot is believed to have occurred to benefit bipedal locomotion (Susman, 1983). The fossilized remains of *Ardipithecus ramidus* (Lovejoy, Latimer, Suwa, Asfaw, & White, 2009), *Australopithecus africanus* (Clarke & Tobias, 1995), *Au. sediba* (Zipfel et al., 2011), *Homo habilis* (Day & Napier, 1964), *H. floresiensis* (Jungers et al., 2009), the Burtele foot bones from Woranso-Mille (Haile-Selassie et al., 2012), and *H. naledi* (Harcourt-Smith et al., 2015) show evidence of feet with variably pronounced arches and both adducted and abducted first metatarsals (MT1), as well as variability in size and skeletal robustness. How, or even if, those foot forms differed functionally remains contentious. The fossil footprints from Laetoli (Leakey & Harris, 1987) and Ileret (Bennett, 2009) have also been used to analyze the gait of individuals and groups. These footprints indicate a more modern foot with adducted MT1 and longitudinal arches, but whether or not the foot that produced these footprints is functionally identical to modern humans also remains a question. Fossil footprints provide, however, key evidence of function, because they demonstrate both the shape of the fleshy foot and the interaction of foot structure with the ground, seen in gait events like heel strike and toe off (e.g. Laetoi (Leakey & Harris, 1987), Ileret (Bennett, 2009), Happisburgh (Ashton et al., 2014), and Willandra Lakes (Webb, Cupper, & Robins, 2006)). Consequently, differences in foot shape in extinct forms imply the potential for differences in the kinetics of walking.

Hypotheses and Goals

Although range of motion of the ankle joint is well documented, most studies incorporated methods that relied on cadaveric feet (Barnett and Napier 1952; Hicks 1953; Manter 1941). While these methods allow us to understand the motion of the isolated ankle, they do not allow us to understand how forces caused by range of motion flow through the talus from the more distal foot to the leg.

Thus, this dissertation offers the following three hypotheses to begin to understand the evolution of the human foot by understand the forces that impact foot morphology. The talus is a prime first suspect to focus this endeavor because it is the only bony connection between the foot and the rest of the body.

- Palpable landmarks on the external surface of the foot, like those used in gait studies, can be used to estimate the in vivo location of the talus.
- Walking while changing direction produces higher side forces that are applied to the human foot than when walking in a straight path.
- The manner in which forces pass through the foot is influenced by the foot's orientation.

The following three goals are required to test these hypotheses: **Goal 1:** Determine if the *in vivo* location of the talus be found using gait external markers typically used in a gait; **Goal 2:** Determine the ground reaction forces applied to the foot when walking in a straight line and when turning. **Goal 3:** Determine if forces aligned in a foot coordinate system differ from those in the world coordinate system in order to inform orthopaedic treatment and rehabilitation.

What follows is an overview of the background literature as it pertains to the functional anatomy of the foot (chapter 2); then three independent studies aimed at exploring the three

hypotheses presented above (chapters 3 through 5); and finally my conclusion for the entire body of work (chapter 6).

Chapters 3 through 5 are formatted as three standalone manuscripts. In chapter 3, the location of external foot markers and internal locations of the talonavicular and posterior subtalar joint were measured on simulated weight-bearing computed tomography (SWCT) scans to determine if the location of the talus could be predicted using the external foot makers. In chapter 4, the XYZ components of the ground reaction force between two walking conditions, walking straight path and walking in a path in which a 90° turn occurs, were compared to evaluate if and how the force profile of a turn is different that the force profile of walking in a straight path. In chapter 5, ground reaction forces are transformed into a newly established coordinate system, the foot coordinate system, to better understand if the forces that pass through the foot are influenced by the orientation of the foot while walking.

Chapter 1: References

Aiello, L., & Dean, C. (2002). *An Introduction to Human Evolutionary Anatomy* (1st ed.). Academic Press.

Ashton, N., Lewis, S. G., Groote, I. De, Duffy, S. M., Bates, M., Bates, R., … Stringer, C. (2014). Hominin footprints from early Pleistocene deposits at Happisburgh, UK. *PLoS ONE*, *9*(2). Retrieved from https://doaj.org/article/c273a830bfb6481e9c5606f8c43f4c4e

Bennett, M. R. (2009). Early Hominin Foot Morphology Based on 1.5-Million-Year-Old Footprints from Ileret, Kenya. *Science*.

Barnett, C. H., & Napier, J. R. (1952). The axis of rotation at the ankle joint in man. *Journal of Anatomy*, *86*(1), 1.

Clarke, R. J., & Tobias, P. V. (1995). Sterkfontein Member 2 Foot Bones of the Oldest South AfricanHominid. *Science*, *269*, 524–621.

Day, M. H., & Napier, J. R. (1964). Fossil Foot Bones. *Nature*, *201*(492), 969–970.

Haile-Selassie, Y., Saylor, B. Z., Deino, A., Levin, N. E., Alene, M., & Latimer, B. M. (2012). A new hominin foot from Ethiopia shows multiple Pliocene bipedal adaptations. *Nature*, *483*(7391), 565–569. https://doi.org/10.1038/nature10922

Harcourt-Smith, W. E. H., & Aiello, L. C. (2004). Fossils, feet and the evolution of human bipedal locomotion. *Journal of Anatomy*, *204*(5), 403–416. https://doi.org/10.1111/j.0021-8782.2004.00296.x

Harcourt-Smith, W. E. H., Throckmorton, Z., Congdon, K. A., Zipfel, B., Deane, A. S., Drapeau, M. S. M., … Desilva, J. M. (2015). The foot of Homo naledi. *Nature Communications*, *6*(1).

Hicks, J. H. (1953). The mechanics of the foot. I. The joints. *Journal of Anatomy*, *87*(4), 345.

Jungers, W. L., Harcourt-Smith, W. E. H., Wunderlich, R. E., Tocheri, M. W., Larson, S. G., Sutikna, T., … Morwood, M. J. (2009). The foot of Homo floresiensis. *Nature*, *459*(7243), 81–84. https://doi.org/10.1038/nature07989

Leakey, M. D., & Harris, J. M. (1987). *Laetoli, A Pliocene site in northern Tanzania*. Oxford [Oxfordshire] : New York: Oxford Oxfordshire : Clarendon Press.

Lovejoy, C. O., Latimer, B., Suwa, G., Asfaw, B., & White, T. D. (2009). Combining prehension and propulsion: the foot of Ardipithecus ramidus. *Science*, *326*(5949), 72e1-8. Retrieved from http://www.ncbi.nlm.nih.gov/entrez/query.fcgi?cmd=Retrieve&db=PubMed&dopt=Citation&list_uids=19810198

Manter, J. T. (1941). Movements of the subtalar and transverse tarsal joints. *Anatomical Record*, *80*(4), 397–410. https://doi.org/10.1002/ar.1090800402

Susman, R. L. (1983). Evolution of the human foot - Evidence from Plio-Pleistocene hominids. *Foot & Ankle: The Official Journal of the American Orthopaedic Foot Society*, *3*(6), 365–376.

Webb, S., Cupper, M. L., & Robins, R. (2006). Pleistocene human footprints from the Willandra Lakes, southeastern Australia. *Journal of Human Evolution*, *50*(4), 405–413.

Zipfel, B., DeSilva, J. M., Kidd, R. S., Carlson, K. J., Churchill, S. E., & Berger, L. R. (2011). The Foot and Ankle of Australopithecus sediba. *Science*, *333*(6048), 1417–1420. https://doi.org/10.1126/science.1202703

Chapter 2: Background

The Functional Anatomy of the Human Foot

The human foot is a dynamic structure that has multiple functions, involved in both locomotion and standing. In an early comprehensive theory of walking and running, it was noted that although the foot changes shape while in contact with the ground, the foot also maintains several points of contact with the ground (E. Weber & Weber, 1836). Biomechanically, the foot behaves like a lever, a rigid bar that rotates around a fulcrum when force is applied (Okuno & Fratin, 2014). When the muscles of the calf (gastrocnemius and soleus) are flexed at toe-off, the Achilles tendon causes plantar flexion (pointing of the toe away from the leg) by pulling up on the calcaneus. Dorsiflexion (bringing the toes closer to the leg) and plantar flexion are motions specific to the foot that are fundamental to propelling the body forward while walking or running. The biomechanical simplification of the human foot as a lever can be misleading, however, as the foot itself is not simply a rigid structure due to the multiple joints found in the foot.

The Human Foot in Primate Context

If the last common ancestor of all apes was a quadruped, a number of skeletal adaptions that are associated with the foot of modern *H. sapiens* are required to have occurred. These adaptions include "an adducted position of the great toe [hallux]" and "lever proportions commensurate with the weight to be lifted and the forces to be transmitted during bipedalism" (Day & Napier, 1964). The two most commonly assumed important developments in hominin bipedal evolution, as it pertains to the foot, are, then, the adduction of the first metatarsal and the presence of the longitudinal arch.

During the toe-off phase of walking, forces of approximately 1.2 times body weight pass (Bowden, 1967) through the medial column (the talus, navicular, cuneiforms, and the first three rays), as the foot pushes off against the ground (Aiello & Dean, 2002). At heel strike similar forces concentrate in the hindfoot. The manner in which the bones and joints of the foot interact with each other can alter how the foot functions (Morton, 1924). The shape of the foot (e.g. the height of the arch) changes as the foot contacts with the ground (Kramer unpublished data), but how this change of shape affects function is unknown.

While it is easy to think of the human foot simply as an ape foot with a longitudinal arch and an adducted first metatarsal, this is not the case. The human foot also is the result of realignments around the subtalar axis (Keith, 1929; Lewis, Ashton, & Holmes, 1981) While the subtalar joint of humans and other apes have some similarities, the axis of the subtalar joint in humans has a steeper dorsoplantar angle than is seen in apes (Aiello & Dean, 2002). This axis also makes a more acute angle with the long axis of the foot than it does in other apes. The decrease seen in this angle is due to the fact that the entire human foot has been medially realigned around this axis. This realignment is thought to have contributed to the first metatarsal's inline orientation with the rest of the foot (Lewis et al., 1981).

The Joints and Their Motion

Excluding the toes, movement within the foot derives from three joints: the ankle, the subtalar, and the midtarsal joints. Analyzing the movement that takes place in these three joints is difficult due to their close proximity to each other (Humphry, 1861). Movement of the talus and calcaneus are restricted due to their shared joint, with opposing surfaces that are shaped like nested curves (Gray, 1858).

The talus is the osteological connection between foot and the leg. The entire weight of the upper body is transmitted through the ankle into the foot during stance, requiring the talus to be, on the one hand, a robust structure. On the other hand, the talus must be able to move relative to the bones with which it articulates (Drake, Vogl, Mitchell, & Gray, 2015). No muscles attach to the talus, so its orientation depends on the bones with which it articulates. The proximal talus connects to the tibial/fibular complex at the ankle, or talocrural joint. The subtalar joint, or talocalcaneal joint, connects the talus to the calcaneus (Figure 2-1). Finally, the head of the talus articulates with the navicular at the talonavicular joint.

The axis of the ankle is also not fixed in a horizontal position. With the foot in dorsiflexion, this axis is inclined inferiorly and laterally. When the foot is plantar flexed, this axis is inclined inferiorly and medially (Figure 2-2) (Barnett & Napier, 1952; Hicks, 1953). During weight-bearing, the axis of the ankle changes and differs significantly between individuals. The axes of plantarflexion, dorsiflexion, pronation, supination, and medial and lateral rotation all coincide at one point in or near the trochlea of the talus (Figure 2-3) (Lundberg, Svensson, Németh, & Selvik, 1989).

The subtalar axis allows rotation within the foot to occur, similar to what happens in a screw. This motion can produce limited rotation of the foot in the form of supination and pronation. This rotation is passive at heel strike and active at toe off. In humans, this axis allows adjustment of the feet to uneven ground (Elftman, 1969; Inman, 1976). The joint rotates at an angle with respect to the axis, causing rotation in a direction oblique to the axis of the joint (Manter, 1941). This motion is also influenced by side; the subtalar joint on the right foot behaves like a right-handed screw while the subtalar joint on the left foot behaves like a left-handed screw. For the joints of the foot, a fixed or stationary joint axis does not work. During

walking, the bodies of the other bones rotate around the talus requiring the orientation of the axes of the corresponding joints to change from one moment to the next during the stride cycle. To compensate for this change in orientation, the mean of all momentary axes can be used to calculate a composite axis. Once the position of the joint axis is known, it is possible to understand the movement and arrangement of the muscles in the region (Klenerman & Wood, 2006). In a living organism, locating the momentary axis of a joint can be problematic. The most reliable method for determining the momentary axes at a joint uses metal pins that are driven into the fixed and moving bones of a cadaveric foot in order to trace a path that could be used to determine the momentary axes (Figure 2-4 and 2-5). These axes can then be applied to living subjects (Manter, 1941).

The axis of the subtalar joint is also not fixed in the horizontal plane. This axis is directed superior and medially as well as anterior instead of directed along the long axis of the foot (Figure 2-4 and 2-5). The direction of this axis is a vestige of the generalized primate form, in which the soles of the feet need to face inward in order to grip tree branches (Aiello & Dean, 2002). It has been shown that the average inclination of the subtalar axis is 42 degrees projected onto the sagittal plane (Figure 2-4) (Elftman & Manter, 1935). This axis also deviates anteriorly and medially from the sagittal plane by 16 degrees. However, individual variation in the axis of the subtalar joint has been shown (Inman, 1976).

The midtarsal joint, sometimes called Chopart's joint, is created by the planar articulation between the calcaneus and the cuboid and the socket joint between the talar head and the navicular (Figure 2-6). This joint complex allows the anterior portion of the foot to pivot relative to the posterior portion of the foot (Elftman, 1960; Morton, 1935) Variation in the height of the longitudinal arch occurs in the midtarsal joint complex (Klenerman & Wood, 2006). The two

axes of the midtarsal joint complex allow the foot to be both pliable at one point and rigid at another during the gait cycle. The axes of these two joints are parallel when the foot is in a neutral stance, making the foot flexible in order to be an effective shock absorber. When the axes of these two joints are not parallel (Figure 2-5), the midtarsal joint is rigid, for instance, at toe-off when the foot is supinated so that it can act as efficient lever for propulsion (Elftman, 1960).

Chapter 2: Appendix

Chapter 2: References

Aiello, L., & Dean, C. (2002). *An Introduction to Human Evolutionary Anatomy* (1st ed.). Academic Press.

Barnett, C. H., & Napier, J. R. (1952). The axis of rotation at the ankle joint in man. *Journal of Anatomy*, *86*(1), 1.

Bowden, R. E. (1967). The functional anatomy of the foot. *Physiotherapy*, *53*(4), 120–126.

Day, M. H., & Napier, J. R. (1964). Fossil Foot Bones. *Nature*, *201*(492), 969–970.

Drake, R. L., Vogl, W., Mitchell, A. W. M., & Gray, H. (2015). *Gray's anatomy for students*. (W. Vogl, A. W. M. Mitchell, & H. Gray, Eds.), *Anatomy for students* (Third edit). Philadelphia, PA: Philadelphia, PA : Churchill Livingstone/Elsevier.

Elftman, H. (1960). The transverse tarsal joint and its control. *Clinical Orthopaedics*, *16*, 41–46.

Elftman, H. (1969). Dynamic structure of the human foot. *Artificial Limbs*, *13*(1), 49–58.

Elftman, H., & Manter, J. (1935). The evolution of the human foot, with especial reference to the joints. *J Anat*, *70*, 56–67.

Gray, H. (1858). *Anatomy, descriptive and surgical*. *Gray's anatomy*. West Stand, London: Parker, John W. & Son.

Hicks, J. H. (1953). The mechanics of the foot. I. The joints. *Journal of Anatomy*, *87*(4), 345.

Humphry, G. M. (1861). *The human foot and the human hand.* Cambridge: Cambridge, Macmillan.

Inman, V. T. (1976). *The joints of the ankle*. Baltimore: Baltimore : Williams & Wilkins.

Keith, A. (1929). The history of the human foot and its bearing on orthopaedic practice. *J Bone Joint Surg.*, *11*, 10–32.

Klenerman, L., & Wood, B. (2006). *The Human Foot: A Companion to Clinical Studies*. London: London: Springer London. https://doi.org/10.1007/b136908

Lewis, O. J., Ashton, E. H., & Holmes, R. L. (1981). Functional morphology of the joints of the evolving foot. *Symposia of the Zoological Society of London*. London: London, United Kingdom: Academic Press.

Lundberg, A., Svensson, O. K., Németh, G., & Selvik, G. (1989). The axis of rotation of the ankle joint. *The Journal of Bone and Joint Surgery. British Volume*, *71*(1), 94. https://doi.org/10.1302/0301-620X.71B1.2915016

Manter, J. T. (1941). Movements of the subtalar and transverse tarsal joints. *Anatomical Record*, *80*(4), 397–410. https://doi.org/10.1002/ar.1090800402

Morton, D. J. (1924). Evolution of the Longitudinal Arch of the Human Foot. *J Bone Joint Surg Am*, *6*, 56–90.

Morton, D. J. (1935). *The Human Foot: Its evolution, physiology and functional disorders*. New York: Columbia Press.

Okuno, E., & Fratin, L. (2014). *Biomechanics of the human body*. (L. Fratin, Ed.). New York: New York : Springer.

Weber, E., & Weber, W. E. (1836). *Mechanics of the human walking apparatus*. (E. (Eduard) Weber, Ed.). Berlin: Berlin.

Chapter 2: List of Figures

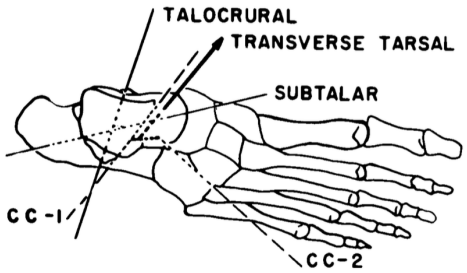

Figure 2-1: The major joints of the ankle (Elftman, 1960).

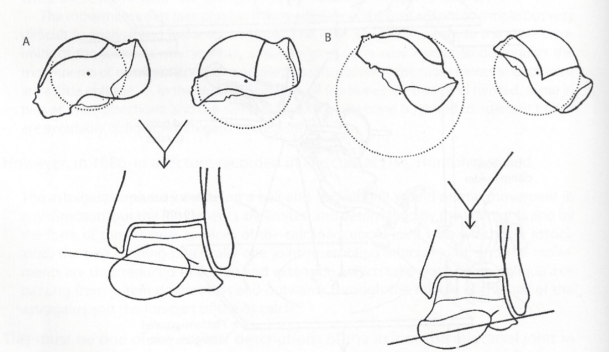

Figure 2-2: A) The profiles of the talus in dorsiflexion. The inclination of the dorsiflexion axis downwards and laterally is obtained by joining the axes of rotation. B) The profiles of the talus in plantarflexion. The inclination of the plantar axis is obtained by joining the centers of rotation (Barnett & Napier, 1952).

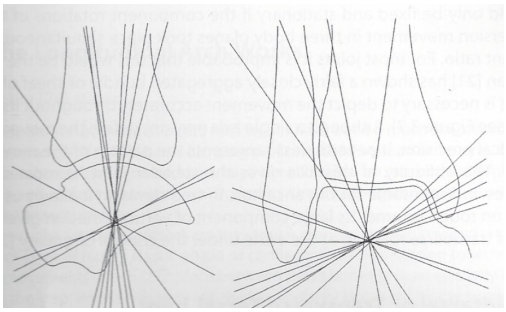

Figure 2-3: Projections of plantarflexion, dorsiflexion, pronation, supination, and medial and lateral rotation meeting at one point of the talus (Lundberg et al., 1989).

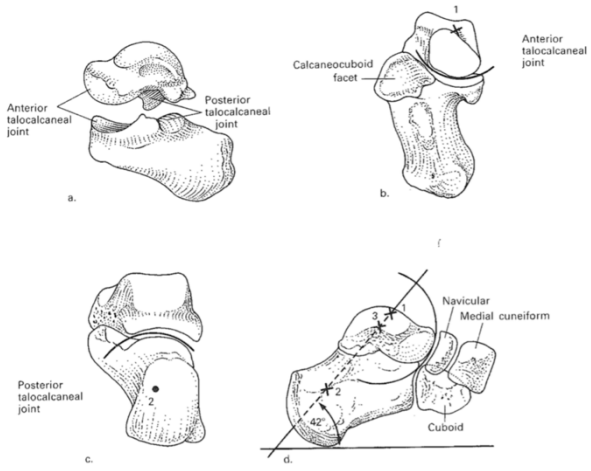

Figure 2-4: The subtalar joint (a) comprises two reciprocal concave and convex articular surfaces, (b) the anterior talocalcaneal joint and (c) the posterior talocalcaneal joint. The subtalar axis passes through the center of the circles (1 and 2) formed by the curved surfaces of the two joints. (d) In the medial view the human subtalar axis also passes through the center of an additional circle 3) formed by the anterior talocalcaneal joint and is inclined by about 42 degrees from the horizontal plane formed by the ground (Aiello & Dean, 2002).

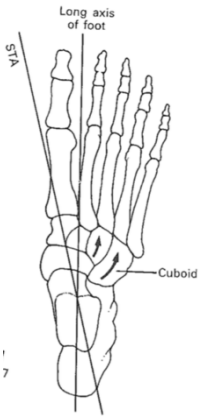

Figure 2-5: The foot in a dorsal view showing the medial orientation of the subtalar axis (STA) (Aiello & Dean, 2002).

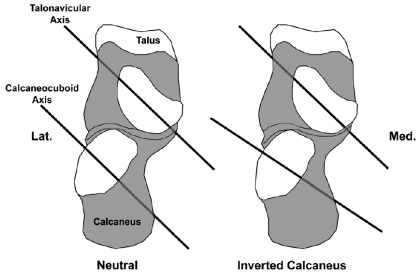

Figure 2-6: The midtarsal joint seen in the frontal plane. The talonavicular and calcaneocuboid axes are parallel when the calcaneus is in eversion (neutral in the figure) and convergent when the subtalar joint is inverted (Inverted calcaneus in the figure) (Blackwood, Yuen, Sangeorzan, & Ledoux, 2005; Elftman, 1960).

Chapter 3: The relationship between external surface markers and the internal location of the talus

Preface

The following chapter is a manuscript in second review (review of revised manuscript) for publication in American Journal of Physical Anthropology under the title "Estimating the *in vivo* location of the talus from external surface landmarks" and authored by Steven G. Lautzenheiser, Adam D. Sylvester, and Patricia A. Kramer

Abstract

Objectives

Finite element analysis (FEA) has gained popularity in anthropological research to connect morphological form to measurable function but requires that loads are applied at appropriate anatomical locations. This is challenging for the ankle because the joint surfaces are not easily determined given their deep anatomical location. While the location of the talonavicular and subtalar joints can be directly determined via medical imaging, regression equations are a common, less invasive method to estimate joint locations from surface anatomy. We propose a regression-based method to locate the *in vivo* positions of the talonavicular and subtalar joints employing three-dimensional (3D) surface markers, such as those used routinely in gait studies.

Materials and Methods

Navicular height was measured on weight-bearing radiographs (WBR) and simulated weight-bearing computed tomography (SWCT) scans to ensure SWCT correctly simulated foot weight-bearing configuration. The location of external foot markers and internal locations of the talonavicular and posterior subtalar joint were measured on each SWCT. Stepwise regression analysis was used to select the external markers that best predicted the three internal locations.

Results

Navicular heights measured on WBR and SWCT scans were not statistically different ($p=0.44$), indicating that SWCTs recreate the weight-bearing position of the foot. The navicular tubercle and medial and lateral malleoli were the best predictors of subtalar and talonavicular joint locations. These palpable anatomical locations explained more variation in internal joint location ($r^2 >0.79$; SEE<3.0 mm) than other landmarks.

Discussion

This study demonstrates that external palpable landmarks can predict the location of the talonavicular and subtalar joints.

Introduction

Finite element analysis (FEA) is a powerful, flexible, and non-invasive method long used in engineering to estimate variables of interest (e.g., stress and strain) and to compare different structures in complex dynamic and static systems (Rayfield, 2007). Advances in computing power and software capabilities have made FEA more accessible to fields outside engineering, such as biology (Jongerius & Lentink, 2010), anthropology (Püschel & Sellers, 2016) and paleontology (Rayfield et al., 2001). Insights gained from FEA have been used successfully within these fields to connect morphological form to measurable function (Nguyen, Pahr, Gross, Skinner, & Kivell, 2014; Smith et al., 2015; Sylvester & Kramer, 2018; Qian Wang et al., 2012).

Human musculoskeletal anatomy can be idealized as a system of linked rigid bodies (i.e., a kinetic chain), in which body segments (e.g., thigh and leg) are modeled as rigid bodies linked together at joints (e.g., the knee). The nature of the system means that motion of one rigid body affects motion of connected (i.e., linked) bodies, and that forces on one side of a joint (e.g., distal femur) are transferred to the other side of the joint (e.g., proximal tibia) (Karandikar & Vargas,

2011). Understanding the kinetic chain assists in locating where loads should be applied at various moments of the gait cycle. Kinetic and kinematics analyses can provide the location of the foot's center of pressure, external marker locations (Figure 1), as well as the ground reaction force. The ground reaction force is transferred to the leg through the bones and joints of the foot using the stiffest path (Qingguo Wang, Pejhan, Wu, & Telichev, 2016). As the talus is the only bony (i.e., stiffest) connection between the foot and the leg, ground reaction forces generated while walking will travel to the talus through two pathways: through the talonavicular joint, when the ground reaction forces are applied to the forefoot (i.e., during late stance) or through the subtalar joint, when the ground reaction forces are transferred from the hindfoot (i.e., from heel strike to foot flat). During midstance, forces are applied through both joints. Since forces applied to the foot always go through the talus it is likely to be subjected to strong selective pressure and hence could be a key to understanding the evolution of the human foot and ankle (Harcourt-Smith & Aiello, 2004).

A critical component of FEA is ensuring that boundary conditions (e.g., forces) are applied to appropriate locations from a functional and anatomical perspective. In order to apply the forces collected in human motion analyses to an FEM of ankle bones, a method is needed to determine the location of these internal joint surfaces without the use of medical imaging. The exact locations of the talonavicular and posterior subtalar joints can, however, only be determined directly via medical imaging, which is costly, inconvenient for participants, and adds unnecessary complexity to analyses (e.g., converting locations within medical image coordinate system to locations in gait lab coordinate system). The goal of this study is, then, to generate regression equations that use palpable landmarks on the external surface of the foot, like those used in gait studies, to estimate the *in vivo* location of the talonavicular and the subtalar joints.

Methods and Materials

Weight-bearing radiographs (WBR) and SWCT scans of healthy feet were retrieved for 16 randomly selected adults, 8 males and 8 females, ages 19-66 years from the database from Harborview Medical Center (Seattle, WA), a Level 1 healthcare facility. WBRs and SWCTs were originally collected for clinical evaluation to rule out the presence of an injury or as comparison views for a contralateral injury (Supporting Information Table 1). Talar dome overlap (Christman, 2003; Montagne, Chevrot, & Galmiche, 1981) was used to classify a lateral radiograph as a true lateral view of the foot.

While imaging techniques, such as compute tomography (CT) scanning, provide the ability to visualize musculoskeletal structures, a major limitation for understanding the position of foot bones from medical images is that they often are not weight bearing. Many clinical orthopaedic procedures attempt to simulate weight bearing by using a device that applies a load to the soles of the feet through a stiff plate that mimics the ground (Hirschmann, Pfirrmann, Klammer, Espinosa, & Buck, 2014; Richter, Seidl, Zech, & Hahn, 2014). For this study, navicular height, a reliable estimate of longitudinal arch height (Hawes, Nachbauer, Sovak, & Nigg, 1992; Razeghi & Batt, 2002; Roth, Roth, Jotanovic, & Madarevic, 2013), was compared between simulated weight-bearing computed tomography (SWCT) and weight-bearing radiographs to determine if SWCT places the bones of the foot into a weight-bearing position. Result of this analysis (discussed in detail below) demonstrate that radiographic and CT-based navicular heights are not different, indicating that the weight-bearing position of the bones of the foot is recreated in the SWCTs.

Palpable landmarks on the external surface of the foot, such as those used in gait analysis for the attachment of markers, were simulated by points located on the skin surface (Figure 2) of the SWCT and the 3D locations of these simulated external landmarks were extracted as 3D

Cartesian coordinates using OsiriX MD (Osirix Viewer, Geneva, Switzerland). Navicular height was measured on both lateral WBR and a sagittally oriented slice in the SWCT image stack (Figure 3). The center of each metatarsal head, the dorsal navicular, heel, navicular tubercle, styloid process of the fifth metatarsal, lateral and medial malleoli, lateral and medial point of the posterior subtalar facet (LPST and MPST), and center of the talar head were measured on either sagittal or transverse sliced SWCT (Table 1). A definition for each external landmark is provided in Appendix 1.

The center of the talar head, used to represent the talonavicular joint, was defined as the location where the long axis of the first metatarsal, a line drawn down the longitudinal axis of the shaft of the first metatarsal, intersects the center of the talar head. On all individuals, this position was measured on both sagittal and transverse sliced SWCT stacks. The sagittal slice used was the one in which the most superior and inferior points of the talar head were visible (Figure 4), while the transverse slice included the most medial and lateral points of the talar head, which were used to determine the center.

To remove variation resulting from foot position during the scan all landmarks of the foot were transformed into a common Cartesian coordinate system. Landmark positions were collected on 11 right and 5 left feet. Left foot landmarks were reflected in order to create a sample of (pseudo-) right feet. The heel marker was used as the origin for the new foot coordinate system and all landmarks within a foot were translated so that the heel marker was positioned at the origin (0,0,0). Each foot was rotated such that the long axis of the foot was aligned with the X-axis. The long axis of the foot was determined by creating a line between the heel marker and the midpoint between 1st metatarsal and 5th metatarsal markers (Figure 5). In

this coordinate system, X represents proximodistal, Y represents mediolateral, and Z represents superioinferior.

Student's t-tests were conducted to compare navicular height in the SWCT and WBR to determine if SWCT simulates true weight-bearing foot configuration. Some landmarks, such as the LPST and MPST, could only be measured on transverse or sagittal slice SWCT. Student's t-tests and a multivariate analysis of covariance (MANCOVA) were conducted on the coordinates of the center of the talar head for feet in which the position could be measured on both transverse and sagittal slices of the SWCT. This was done to determine if landmarks found only on the transverse slices could be used in the analyses of landmarks found only on sagittal slices. MANCOVA analyses did not indicate differences in measurements, so the analyses are not presented.

Linear regression was used to determine the ability of the locations of the external landmarks to predict the location of the center of the talar head. Stepwise regression was used to determine which external landmarks produced a best fit model for each of the three talar point's X, Y, and Z coordinates. All statistics were completed in Stata (V15, StataCorp, College Station, TX) using an alpha value of 0.05. This study was approved by the Institutional Review Board of the University of Washington.

Results

Mean navicular height on WBR were not statistically different ($p=0.44$) from that obtained from the SWCT scans: 7.17 cm vs 7.13 cm. Mean X, Y, and Z locations of the center of the talar head measured on sagittal SWCT scans are not significantly different from those obtained from transverse SWCT scans in all three coordinates: X 80.04 mm vs 77.27 mm ($p=0.70$); Y 26.68 vs. 26.35 ($p=0.95$); and Z 40.74 vs. 42.12 ($p= 0.89$).

Linear regressions of each landmark's X, Y, and Z coordinates indicated that the lateral and medial malleoli, dorsal navicular, and navicular tubercle are predictive of the center of the talar head and the medial and lateral posterior subtalar points. The centers of the metatarsal heads 2-4 and styloid process of the 5th metatarsal were predictive of only the X position of the three internal points and, therefore, were not included in stepwise regression (Table 2; Supportive Information Table 2). The dorsal navicular was not included in the stepwise regression as this point might not be as reliable when the foot rotates about the ankle during the gait cycle due to the movement of the underlying soft tissues.

Stepwise regression revealed that the navicular tubercle and both (lateral and medial) malleoli explained more of the variation of the center of the talar head (r^2 0.66-0.92; SEE: 1.7-2.3mm) and the medial (r^2 0.56-0.82; SEE: 2.2-3.2mm) and lateral (r^2 0.76-0.85; SEE: 1.0-1.9mm) points of posterior subtalar facet than did other external locations (Table 3; Figures 6-8). Adding sex and age to the stepwise regression did not improve the fit of the model.

Discussion

Our results demonstrate that the location of the talonavicular and posterior subtalar joints can be predicted reliably from the location of external markers on the navicular tubercle and lateral and medial malleoli. Due to their close proximity to the talus, it is unsurprisingly that these three bony landmarks were predictive of the location of the joints. The SWCTs used in this study were acquired using conventional medical CT instruments resulting in thicker slice than a high resolution CT. The resolution of the SWCTs could explain why the points for the talonavicular and lateral posterior subtalar joints had higher predictive value compared to the medial posterior subtalar joint. In a living human subject, it is easier to find the center of the talonavicular joint than either of the two subtalar points. Of them, the medial is more difficult

than the lateral to identify. Nonetheless, the degree to which variation in internal position of the joints was predicted by external landmarks is encouraging for future FEA of the talus.

Although the feet in this study were unmoving, in gait studies, the foot moves and the position of markers can be affected by the movement of soft tissue, including the skin. An example of this potential problem is the dorsal navicular marker. While a statistically significant predictor of the location of the three joints of interest in this study, the dorsal navicular marker might move more due to skin slippage compared to other markers. The lateral and medial malleoli and navicular tubercle are relatively close to the skin with no intervening tendons, so they have less soft tissue movement. Additionally, they are easily palpable.

The reported regression equations can thus be used to locate the *in vivo* locations of the talonavicular and posterior subtalar joints using data collected from traditional kinematic gait analyses or clinical examination. While further analyses are required, these same techniques are likely to predict if the *in vivo* locations of other joints of the foot, such as the calcaneocuboid joint.

Chapter 3: Appendix

Chapter 3: References

Aiello, L., & Dean, C. (2002). *An Introduction to Human Evolutionary Anatomy* (1st ed.). Academic Press.

Bassett, D. R., Schneider, P. L., & Huntington, G. E. (2004). Physical Activity in an Old Order Amish Community. *Medicine & Science in Sports & Exercise*, *36*(1), 79–85. https://doi.org/10.1249/01.MSS.0000106184.71258.32

Bassett, D. R., Wyatt, H. R., Thompson, H., Peters, J. C., & Hill, J. O. (2010). Pedometer-Measured Physical Activity and Health Behaviors in U.S. Adults. *Medicine & Science in Sports & Exercise*, *42*(10), 1819–1825. https://doi.org/10.1249/MSS.0b013e3181dc2e54

Bischof, J. E., Abbey, A. N., Chuckpaiwong, B., Nunley, J. A., & Queen, R. M. (n.d.). Three-dimensional ankle kinematics and kinetics during running in women. *Gait Posture*, *31*(4), 502–505. https://doi.org/S0966-6362(10)00063-9 [pii]10.1016/j.gaitpost.2010.02.010

Bowden, R. E. (1967). The functional anatomy of the foot. *Physiotherapy*, *53*(4), 120–126.

Cavagna, G. A., Thys, H., & Zamboni, A. (1976). The sources of external work in level walking and running. *The Journal of Physiology*, *262*(3), 639–657. https://doi.org/10.1113/jphysiol.1976.sp011613

Cavanagh, P. R., & Lafortune, M. A. (1980). Ground reaction forces in distance running. *Journal of Biomechanics*, *13*(5), 397–406. https://doi.org/10.1016/0021-9290(80)90033-0

Chang, Y. H., Huang, H. W., Hamerski, C. M., & Kram, R. (2000). The independent effects of gravity and inertia on running mechanics. *The Journal of Experimental Biology*, *203*(Pt 2), 229.

Chehab, F. F., Pontzer, H., Raichlen, D. A., Wood, B. M., Mabulla, A. Z. P., Racette, S. B., &

Marlowe, F. W. (2012). Hunter-Gatherer Energetics and Human Obesity. *PLoS ONE*, *7*(7), e40503. https://doi.org/10.1371/journal.pone.0040503

Christman, R. A. (2003). *Foot and ankle radiology*. St. Louis: Churchill Livingstone.

Frost, H. M. (1982). Mechanical determinants of bone modeling. *Metabolic Bone Disease & Related Research*, *4*(4), 217.

Hader, K., Palazzi, D., & Buchheit, M. (2015). Change of direction speed in soccer: how much braking is enough?(Original scientific paper). *Kinesiology*, *47*(1), 67.

Harcourt-Smith, W. E. H., & Aiello, L. C. (2004). Fossils, feet and the evolution of human bipedal locomotion. *Journal of Anatomy*, *204*(5), 403–416. https://doi.org/10.1111/j.0021-8782.2004.00296.x

Hawes, M. R., Nachbauer, W., Sovak, D., & Nigg, B. M. (1992). Footprint Parameters as a Measure of Arch Height. *Foot & Ankle International*, *13*(1), 22–26. https://doi.org/10.1177/107110079201300104

Hirschmann, A., Pfirrmann, C. W. A., Klammer, G., Espinosa, N., & Buck, F. M. (2014). Upright Cone CT of the hindfoot: Comparison of the non-weight-bearing with the upright weight-bearing position. *European Radiology*, *24*(3), 553–558. https://doi.org/10.1007/s00330-013-3028-2

Huang, T.-W. P., & Kuo, A. D. (2014). Mechanics and energetics of load carriage during human walking. *The Journal of Experimental Biology*, *217*(Pt 4), 605. https://doi.org/10.1242/jeb.091587

Jin, J. (2014). Running Injuries. *JAMA*, *312*(2), 202. https://doi.org/10.1001/jama.2013.283011

Jongerius, S. R., & Lentink, D. (2010). Structural Analysis of a Dragonfly Wing. *Experimental Mechanics*, *50*(9), 1323–1334. https://doi.org/10.1007/s11340-010-9411-x

Karandikar, N., & Vargas, O. O. O. (2011). Kinetic Chains: A Review of the Concept and Its Clinical Applications. *PM&R*, *3*(8), 739–745. https://doi.org/10.1016/j.pmrj.2011.02.021

Marlowe, F. W. (2005). Hunter-gatherers and human evolution. *Evolutionary Anthropology: Issues, News, and Reviews*, *14*(2), 54–67. https://doi.org/10.1002/evan.20046

Minetti, A. E. (1995). Optimum gradient of mountain paths. *Journal of Applied Physiology*, *79*(5), 1698–1703. https://doi.org/10.1152/jappl.1995.79.5.1698

Montagne, J., Chevrot, A., & Galmiche, J.-M. (1981). *Atlas of foot radiology*. New York: Masson Pub. USA.

Morio, C., Lake, M. J., Gueguen, N., Rao, G., & Baly, L. (2009). The influence of footwear on foot motion during walking and running. *Journal of Biomechanics*, *42*(13), 2081–2088. https://doi.org/10.1016/J.JBIOMECH.2009.06.015

Morris, J. M. (1977). Biomechanics of the foot and ankle. *Clinical Orthopaedics and Related Research*, (122), 10–17.

Nguyen, N. H., Pahr, D. H., Gross, T., Skinner, M. M., & Kivell, T. L. (2014). Micro-finite element (μFE) modeling of the siamang (Symphalangus syndactylus) third proximal phalanx: The functional role of curvature and the flexor sheath ridge. https://doi.org/10.1016/j.jhevol.2013.12.008

Nilsson, J., & Thorstensson, A. (1989). Ground reaction forces at different speeds of human walking and running. *Acta Physiologica Scandinavica*, *136*(2), 217–227. https://doi.org/10.1111/j.1748-1716.1989.tb08655.x

Orien, W. P., Weed, J. H., & Root, M. L. (1977). *Normal and abnormal function of the foot*. (W. P. Orien & J. H. Weed, Eds.) (1st ed.). Los Angeles: Los Angeles : Clinical Biomechanics Corp.

Püschel, T. A., & Sellers, W. I. (2016). Standing on the shoulders of apes: Analyzing the form and function of the hominoid scapula using geometric morphometrics and finite element analysis. *American Journal of Physical Anthropology*, *159*(2), 325–341. https://doi.org/10.1002/ajpa.22882

Rayfield, E. J., Norman, D. B., Horner, C. C., Horner, J. R., Smith, P. M., Thomason, J. J., & Upchurch, P. (2001). Cranial design and function in a large theropod dinosaur. *Nature*, *409*(6823), 1033–1037. https://doi.org/10.1038/35059070

Razeghi, M., & Batt, M. E. (2002). Foot type classification: a critical review of current methods. *Gait & Posture*, *15*(3), 282–291. https://doi.org/10.1016/S0966-6362(01)00151-5

Richter, M., Seidl, B., Zech, S., & Hahn, S. (2014). PedCAT for 3D-imaging in standing position allows for more accurate bone position (angle) measurement than radiographs or CT. *Foot and Ankle Surgery*, *20*(3), 201–207. https://doi.org/10.1016/j.fas.2014.04.004

Roth, S., Roth, A., Jotanovic, Z., & Madarevic, T. (2013). Navicular index for differentiation of flatfoot from normal foot. *International Orthopaedics*, *37*(6), 1107–1112. https://doi.org/10.1007/s00264-013-1885-6

Rue, M. J., & Kramer, P. A. (2017). Minimal energetic expenditure of women walking burdened on gradients in urban environments. *American Journal of Human Biology*, *29*(1), n/a-n/a. https://doi.org/10.1002/ajhb.22907

Ruff, C., Holt, B., & Trinkaus, E. (2006). Who's afraid of the big bad Wolff?: "Wolff's law" and bone functional adaptation. *American Journal of Physical Anthropology*, *129*(4), 484–498. https://doi.org/10.1002/ajpa.20371

Scott, S. H., & Winter, D. A. (1990). Internal forces of chronic running injury sites. *Medicine and Science in Sports and Exercise*, *22*(3), 357.

Smith, A. L., Benazzi, S., Ledogar, J. A., Tamvada, K., Pryor Smith, L. C., Weber, G. W., … Strait, D. S. (2015). Biomechanical Implications of Intraspecific Shape Variation in Chimpanzee Crania: Moving Toward an Integration of Geometric Morphometrics and Finite Element Analysis. *The Anatomical Record*, *298*(1), 122–144. https://doi.org/10.1002/ar.23074

Stokes, I. A., Hutton, W. C., & Stott, J. R. (1979). Forces acting on the metatarsals during normal walking. *J Anat*, *129*(Pt 3), 579–590.

Sylvester, A. D., & Kramer, P. A. (2018). Young's Modulus and Load Complexity: Modeling Their Effects on Proximal Femur Strain. *The Anatomical Record*, *301*(7), 1189–1202. https://doi.org/10.1002/ar.23796

Voloshina, A. S., Kuo, A. D., Daley, M. A., & Ferris, D. P. (2013). Biomechanics and energetics of walking on uneven terrain. *Journal of Experimental Biology*, *216*(21), 3963–3970. https://doi.org/10.1242/jeb.081711

Wang, Qian, Wood, S. A., Grosse, I. R., Ross, C. F., Zapata, U., Byron, C. D., … Strait, D. S. (2012). The Role of the Sutures in Biomechanical Dynamic Simulation of a Macaque Cranial Finite Element Model: Implications for the Evolution of Craniofacial Form. *The Anatomical Record: Advances in Integrative Anatomy and Evolutionary Biology*, *295*(2), 278–288. https://doi.org/10.1002/ar.21532

Wang, Qingguo, Pejhan, K., Wu, C. Q., & Telichev, I. (2016). Load Transfer Index for Composite Materials. *Volume 9: Mechanics of Solids, Structures and Fluids*, V009T12A009. https://doi.org/10.1115/imece2015-51176

Wilson, A. M., Hubel, T. Y., Wilshin, S. D., Lowe, J. C., Lorenc, M., Dewhirst, O. P., … West, T. G. (2018). Biomechanics of predator–prey arms race in lion, zebra, cheetah and impala.

Nature, *554*(7691), 183–188. https://doi.org/10.1038/nature25479

Chapter 3: List of Tables

CT View	Palpable External	Internal point
Sagittal Slice	Heel	Center of the talar head
	Dorsal Navicular	
	Centers of MT1-MT5 Heads	
Transverse Slice	Navicular Tubercle	Lateral point of the posterior subtalar facet
	Styloid process of the fifth metatarsal	Medial point of the posterior subtalar facet
	Lateral malleolus	Center of the talar head
	Medial malleolus	

Table 1: All landmarks (palpable external and internal points) used measured in this study divided into what CT slice (sagittal or transverse) was used to measure their location.

	Talar Head						Medial Posterior Subtalar Facet						Lateral Posterior Subtalar Facet					
	X		Y		Z		X		Y		Z		X		Y		Z	
External Marker	**r^2**	**p-value**	**r^2**	**p-value**	**r^2**	**p-value**	**r^2**	**p-value**	**r^2**	**p-value**	**r^2**	**p-value**	**r^2**	**p-value**	**r^2**	**p-value**	**r^2**	**p-value**
Navicular Tubercle	0.79	<0.001	0.59	<0.001	0.84	<0.001	0.53	0.001	0.45	0.004	0.64	<0.001	0.57	0.001	0.47	0.003	0.57	0.001
Medial Malleolus	0.65	<0.001	0.66	<0.001	0.55	0.001	0.66	<0.001	0.56	0.001	0.64	<0.001	0.60	<0.001	0.52	0.002	0.50	0.002
Lateral Malleolus	0.60	<0.001	0.54	0.001	0.53	0.001	0.48	0.003	0.47	0.003	0.55	0.001	0.74	<0.001	0.85	<0.001	0.59	0.001

Table 2: Correlations of the navicular tubercle, medial and lateral malleolus to talar joint position. X (Proximodistal), Y(mediolateral) and Z (superioinferior) refer to the axes of the foot coordinate system.

Predictive Equation		R^2	SEE (mm)
Talar Head	X = 23.6 + 0.51*Navicular Tubercle(X) + 0.48*Lateral Malleolus(X)	0.91	1.7
	Y = -14.3 + 0.69*Medial Malleolus(Y)	0.66	2.3
	Z = 4.5 + 0.70*Navicular Tubercle(Z) + 0.30* Lateral Malleolus(Z)	0.92	1.7
Medial Posterior Subtalar Facet	X = 1.9 + 0.75*Medial Malleolus(X)	0.66	1.8
	Y = -6.0 + 0.57*Medial Malleolus(Y)	0.56	3.0
	Z = -5.9 + 0.41*Navicular Tubercle(Z) + 0.50* Medial Malleolus(Z)	0.82	2.3
Lateral Posterior Subtalar Facet	X= 4.9 + 0.68*Lateral Malleolus(Y) + 0.28* Navicular Tubercle(X)	0.85	1.9
	Y = 14.9 + 0.87*Lateral Malleolus(Y)	0.85	1.5
	Z = -3.1 + 0.38*Navicular Tubercle(Z) + 0.36*Lateral Malleolus(Z)	0.76	1.0

Table 3: Predictive equations for locating the three talar joints. X (Proximodistal), Y(mediolateral) and Z (superioinferior) refer to the axes of the foot coordinate system.

Chapter 3: List of Figures

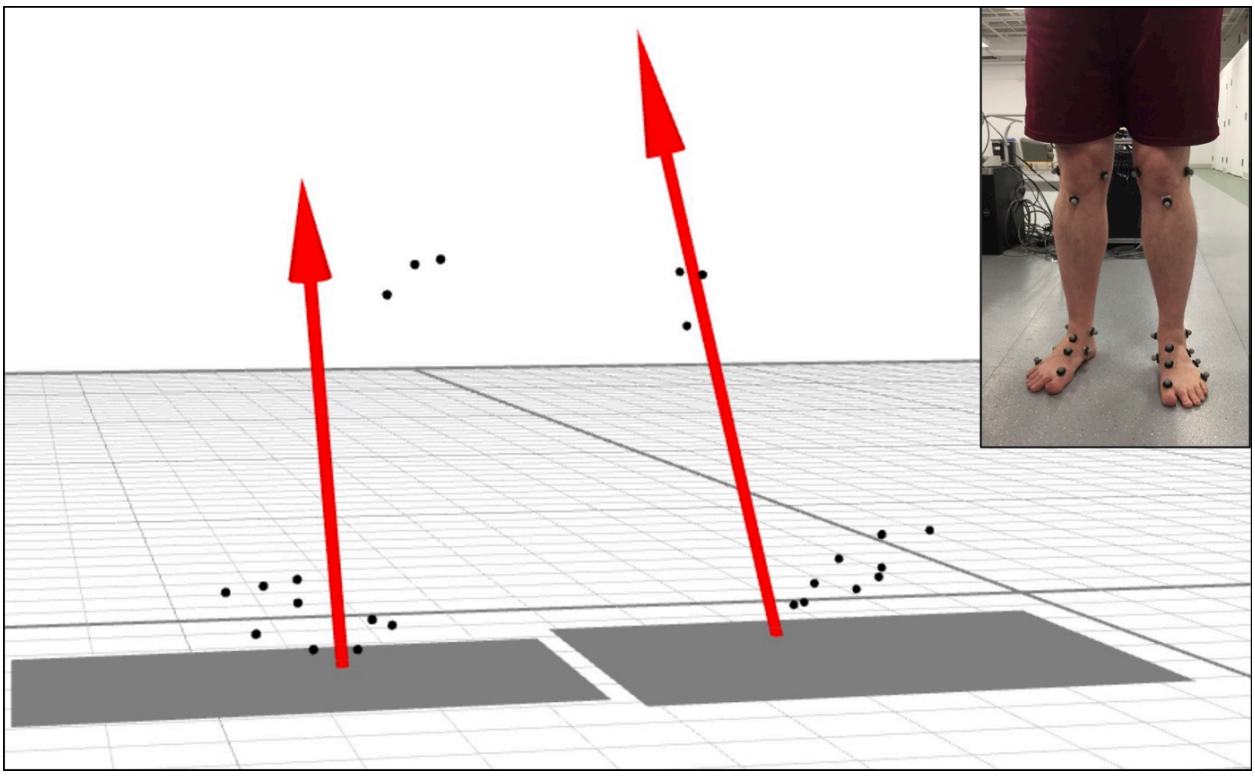

Figure 1: Typical gait analysis. Participant with markers and the virtual representation of the participant during a walking trial.

Figure 2: Simulated external markers placed on the skin on a SWCT representing the dorsal navicular and the center of the second metatarsal head. Markers in image are sized to be visible and are not to scale.

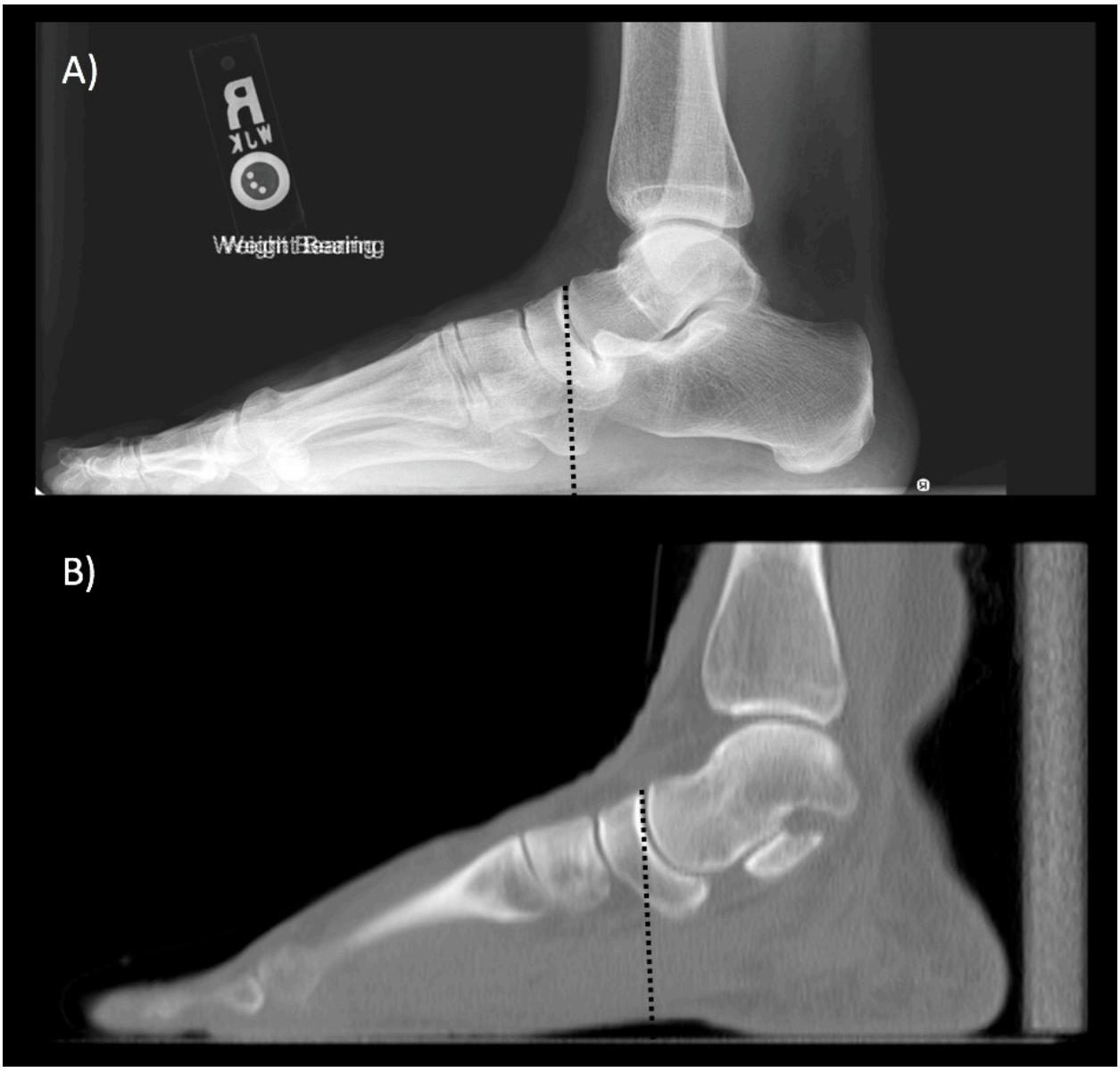

Figure 3: Navicular height, represented by the dotted black on weight-bearing radiograph (A) and solid white lines on a SWCT (B), for the same participant.

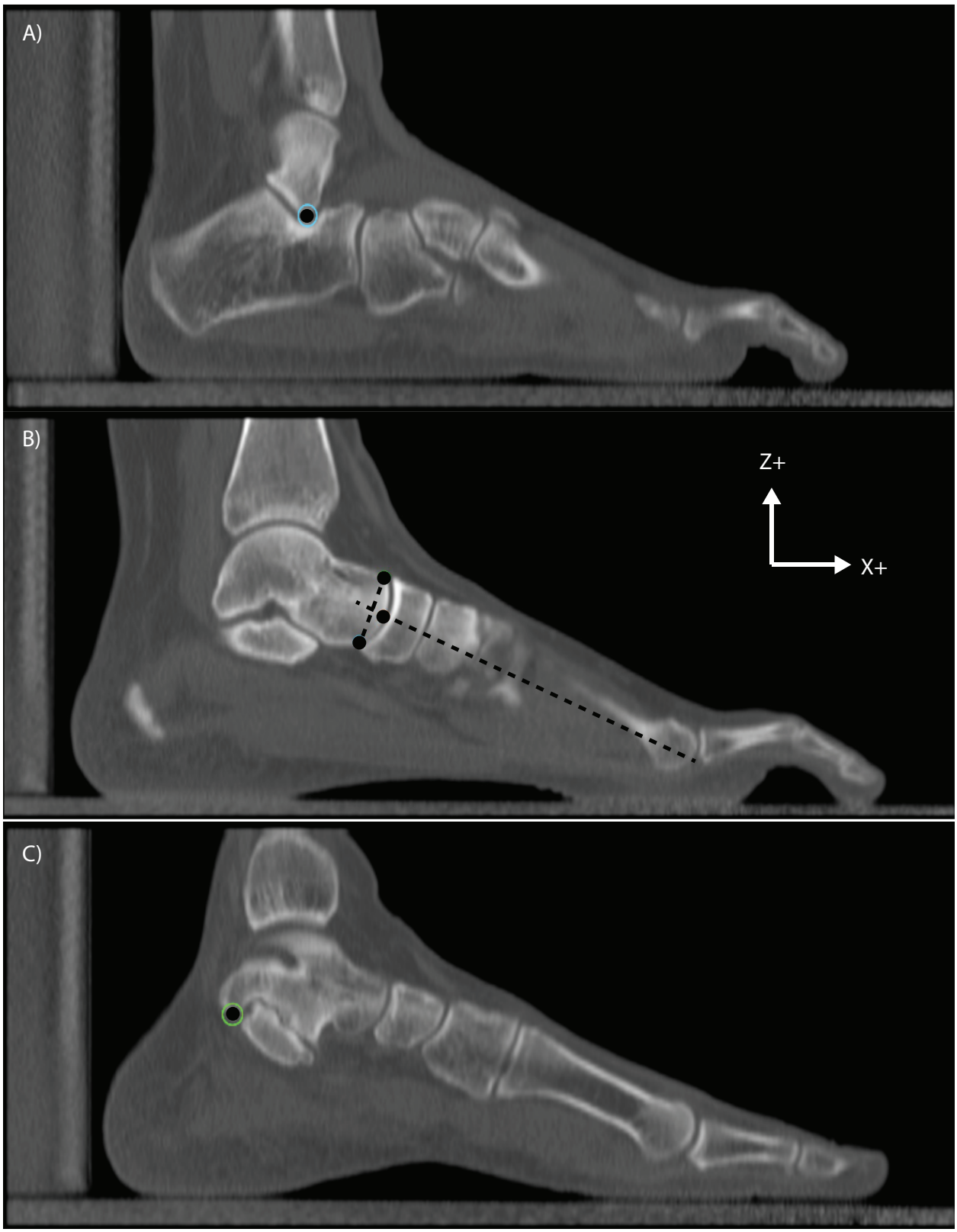

Figure 4: Location for the three *in vivo* talar points on a sagittal sliced SWCT: (A) the lateral posterior subtalar facet, (B) The center of the talar head, and C) The medial posterior subtalar. Markers in image are not to scale.

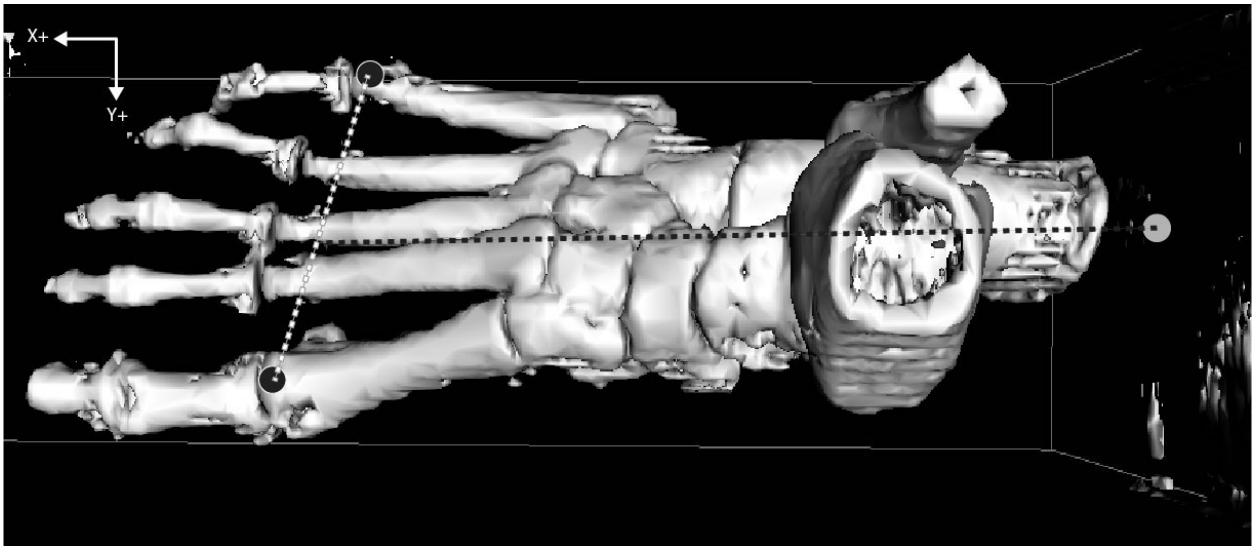

Figure 5: Virtual reconstruction of the foot from SWCT. The long axis of the foot (black dotted line) is created using the midpoint between markers for the 1st and 5th metatarsals and the heel. Markers in image are not to scale.

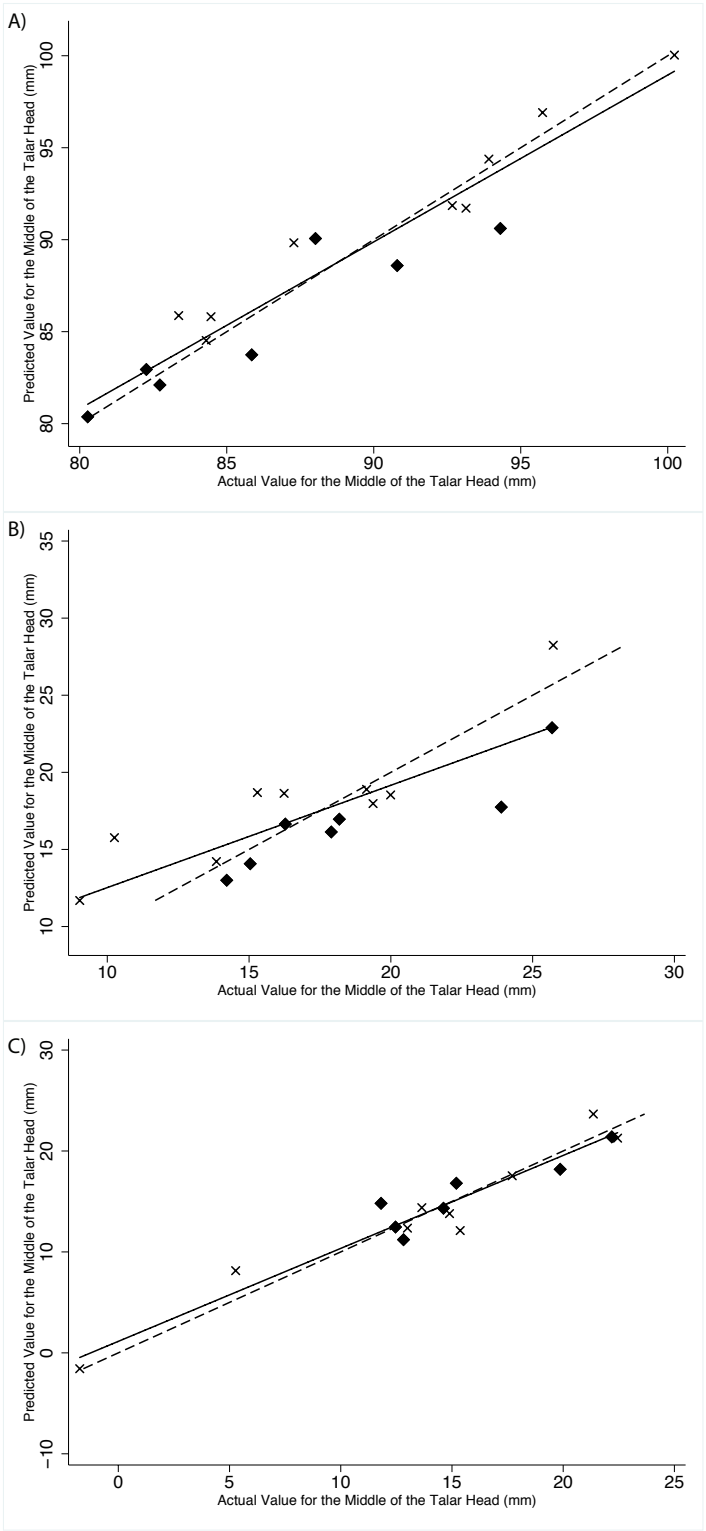

Figure 6: The (A) X-location (B) Y-location and (C) Z-location in millimeters of the predicted location of the center of the talar head over the measured location of the center of the talar head. Solid line is the best fit line and dotted line is the y=x line. Diamonds are feet that were imaged in order to rule out injury while X's are feet that were imaged as comparison for an injured foot.

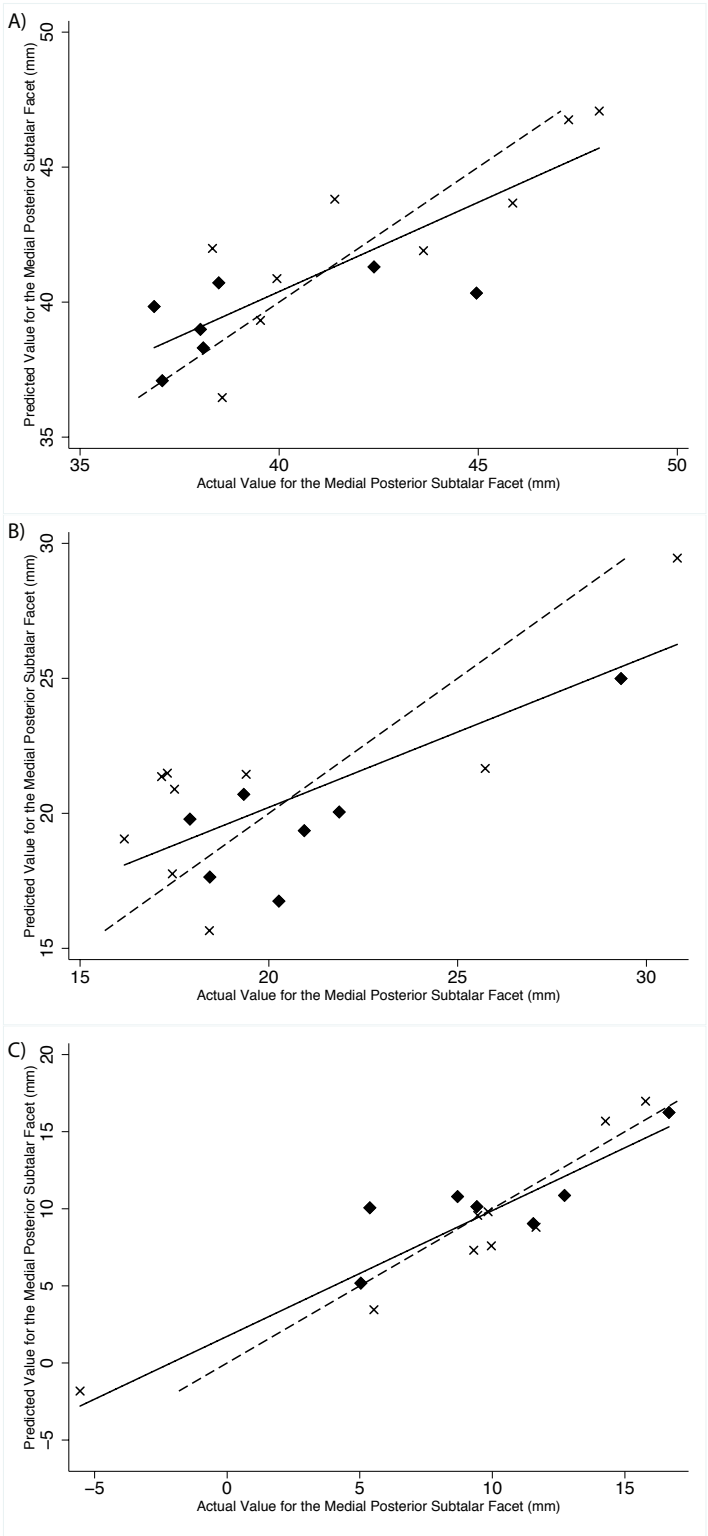

Figure 7: The (A) X-location (B) Y-location and (C) Z-location in millimeters of the predicted location of the medial posterior subtalar facet over the measured location of the medial posterior subtalar facet. Solid line is the best fit line and dotted line is the y=x line. Diamonds are feet that were imaged in order to rule out injury while X's are feet that were imaged as comparison for an injured foot.

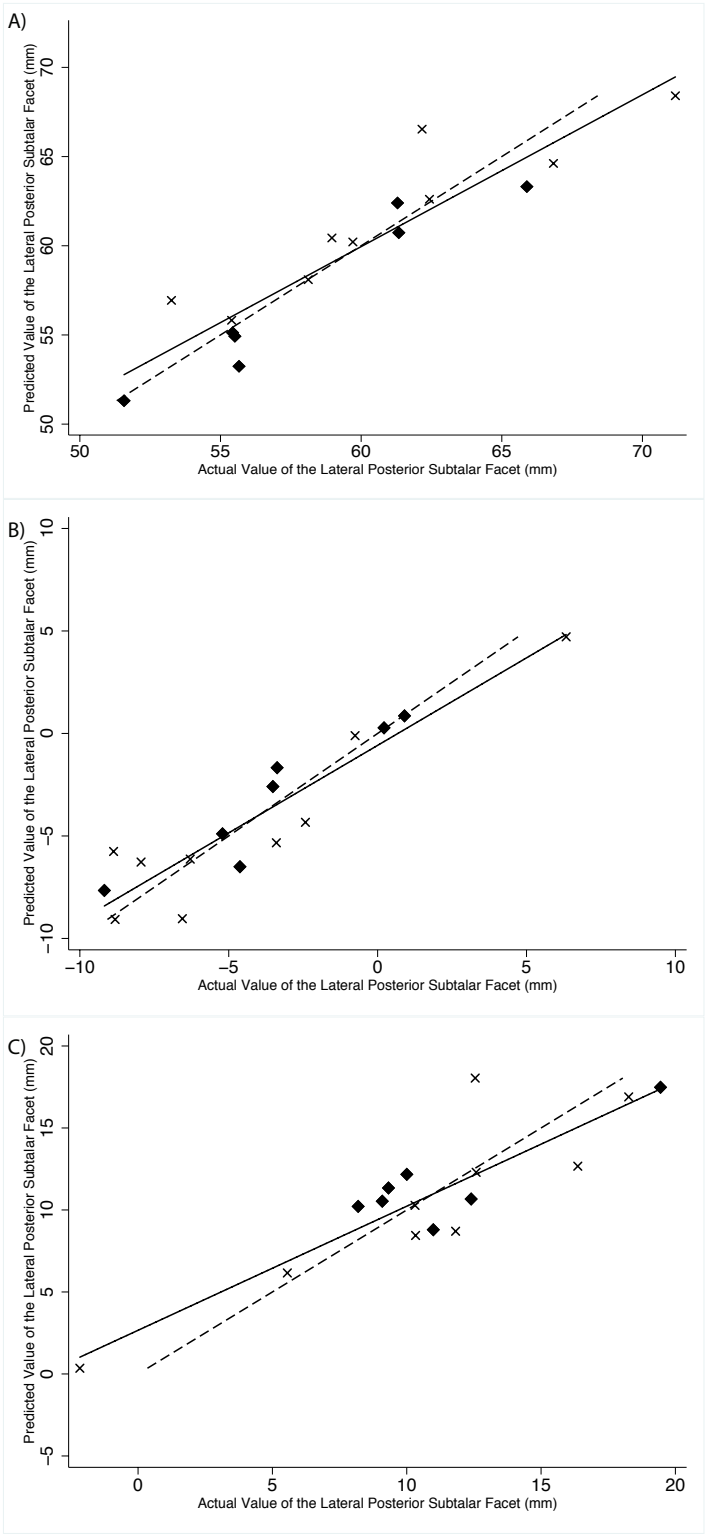

Figure 8: The (A) X-location (B) Y-location and (C) Z-location in millimeters of the predicted location of the lateral posterior subtalar facet over the measured location of the lateral posterior subtalar facet. Solid line is the best fit line and dotted line is the y=x line. Diamonds are feet that were imaged in order to rule out injury while X's are feet that were imaged as comparison for an injured foot.

Chapter 4: Force differences in directional changes

Preface

The following chapter is a manuscript that will be submitted for Gait and Posture in July 2019 authored by Steven G. Lautzenheiser, Adam D. Sylvester, and Patricia A. Kramer.

Abstract

Background: When walking, humans alter the path in which they are traveling for various reasons, such as avoiding obstacles in their path. Researcher often overlook how important turning is, despite how common this phenomenon occurs, when investigating how the body responds to the forces associated with locomotion.

Research question: The purpose of this study was to compare XYZ components of the ground reaction force between two walking conditions: walking straight path and walking in a path in which a 90° turn occurs.

Methods: (9 males 11 females) adults (ages 19-55) participated in this study. Ground reaction forces were collected as participants walked at their self-selected normal velocity in straight and 90° turning conditions.

Results: Changing directions while walking greatly affects the magnitude of the applied forces to the body. During both the braking and propulsion phases of the stance, the magnitude of both forward and side forces are higher in a turn than when walking in a straight path.

Significance: As turning is so common, understanding how directional change affects the applied forces to the body is an important component to furthering our understand of bipedal locomotion

Introduction

Bipedal locomotion is, arguably, the defining characteristic of the human lineage, and humans spend a substantial amount of time moving through their environment during daily life (Bassett, Schneider, & Huntington, 2004; Bassett, Wyatt, Thompson, Peters, & Hill, 2010; Chehab et al., 2012; Marlowe, 2005) . Consequently, the energetics and biomechanics of bipedal locomotion has been extensively investigated. Typically, however, these analyses are conceived to evaluate a linear behavior that allows an individual to move from one point to another and can, therefore, often be replicated on a treadmill. Locomotion is more, however, than simply displacing the body through space in a straight line. In order to fully understand this complex phenomenon, researchers need to take into account additional parameters that affect normal gait when describing the locomotor process. Appreciating the effect of changes in speed (Bischof, Abbey, Chuckpaiwong, Nunley, & Queen, n.d.; Cavanagh & Lafortune, 1980; Morio, Lake, Gueguen, Rao, & Baly, 2009; Stokes, Hutton, & Stott, 1979), terrain (Rue & Kramer, 2017; Voloshina, Kuo, Daley, & Ferris, 2013) and burden status (Huang & Kuo, 2014; Rue & Kramer, 2017), to list a small number of parameters, has substantially altered our understanding of human locomotion.

These previous studies were, however, limited to an evaluation of individuals moving in a straight path, but people change their direction of travel often and for various reasons, including terrain perturbations (Minetti, 1995) and interactions with other individuals (Hader, Palazzi, & Buchheit, 2015; Wilson et al., 2018). In fact, it is unusual for an individual to walk without needing a directional change at some point in their travels. This study seeks, consequently, to reveal how turning affects the magnitude and orientation of the ground reaction force (GRF) in walking adults.

When walking in a straight path, while one foot contacts the ground, the other foot swings forward in a pendular motion in order to conserve energy (Cavagna, Thys, & Zamboni, 1976). When an individual changes direction, the body needs to be redirected from its original path, upsetting the pendular motion of the lower limb. This redirection requires alteration of the forces generated during the braking and propulsive phases of stance to accommodate this directional change. At a minimum, a force that is applied at an angle to the original direction of travel, and parallel to the new direction, is required to redirect the individual. The body must be able to accommodate alteration to the applied forces.

The foot is a mechanically complex structure, with its principle role to act as the only interface between the individual and the substrate. To do this, the foot must perform multiple functions in the stance phase of the gait cycle: provide shock absorption as the heel strikes the ground (Morris, 1977; Orien, Weed, & Root, 1977); function as a rigid lever during the propulsive phase of the stance (Morris, 1977); and accommodate to uneven or unstable terrain. These functions create a chain reaction among the multiple joints of the foot (Aiello & Dean, 2002). The human foot is directly affected by the alteration of forces associated with directional changes.

Mechanical forces play a critical role in bone function and development. The mature shape of each bone is influenced by the forces to which it is exposed, as bone can be resorbed or added in response to load (Frost, 1982). Bones and joints, particularly those of the foot, are not symmetric, making the direction that a force is applied as important as the force's magnitude. For example, a bone may be strong in compression (resulting from axial forces), but less capable in bending (resulting from shear forces) (Ruff, Holt, & Trinkaus, 2006). To evaluate the

structural integrity of the bones and joints of the foot, the magnitude and direction of the forces applied to it must be known accurately.

The two periods in the stance phase where the forces that travel through the foot are highest are when the foot first makes initial contact with the ground (Morris, 1977; Orien et al., 1977) and when the foot pushes off against the ground (Morris, 1977). The GRF produced while walking in a straight path can be divided into three components: vertical, forward, and side. Vertical forces react the gravitational forces of the body as the individual collides with the substrate while walking. Vertical forces usually have the largest magnitude of the three components. During the propulsive phase of walking in a straight line, vertical forces equal to approximately 1.2 times body weight (Bowden, 1967) pass through the foot as it pushes off against the ground. These forces are increased to 1.5-2 times body weight in long distance running in a straight path (Nilsson & Thorstensson, 1989). Forward forces both brake, in early stance, and propel, in late stance, the individual and are approximately .25 times body weight (Nilsson & Thorstensson, 1989). Side forces are the smallest component of the three, produced to balance and stabilize the body (Figure 1).

To our knowledge no previous study has investigated the GRF associated with changing the direction of travel in human walking. Hence, the main objective of the present investigation is to compare the GRF produced while walking in a straight path to the GRF generated in making a 90º turning, with particular attention paid to changes in force magnitude among the GRF components. We hypothesize that walking while changing direction produces higher side forces that are applied to the human foot than when walking in a straight path.

Methods

Subject population

Twenty healthy participants (9 females, 11 males) were recruited for this study. Body mass (kg) and stature (cm) were measured for each participant (Table 1). All participants were free from self-reported lower-limb injuries. The University of Washington's Institutional Review Board approved all procedures of this study (IRB#: 1STUDY00001125).

Experimental Protocol

Kinetic data were measured on individuals using a four-force plate (Kistler, Switzerland), 10-camera motion capture system (Qualisys, Sweden) in the Amplifying Movement & Performance (AMP) laboratory of the University of Washington. The force plates are designated A-D in the direction of travel (Figure 2). Thirteen infrared-reflective markers (5mm hemispherical markers) were affixed to anatomical landmarks of the foot, ankle, and calf (Figure 2a; Table 2).

Using their self-selected normal pace, participants walked unshod the length of the gait lab. Two walking conditions were explored for this study. In the first condition, participants walked in a straight path contacting the surface of each force plate with a single foot. Trials with multiple feet on a particular force plate or a foot that exceeded the force plate margins were discarded and immediately redone. The second condition was a 90° turn to the right where the participant contacted the force plates A and C with their left foot (Figure 2c) and force plate B with their right foot. Five trials for each condition were obtained. GRF components were evaluated for three steps of a trial using the first three force plates A-C (Figure 1b). In the straight path condition, the participants walked across all force plates. In the turning conditions, participants walked in a straight path across force plates A and B and turned on force plate C.

Marker data and the GRF were collected at 120 Hz and the raw marker data were filtered at 10 Hz with a 4^{th} order, low pass zero-lag Butterworth filter. Calibration of the system yielded a limitation in its fidelity for marker data of 1mm and force data of ±2.5N for the forward (X), ±5N side (Y), and ±25N vertical (Z).

Definition of key variables

Force data from plates A and C were analyzed for this study. The GRF components in the forward (in the direction of initial travel, X), lateral (to the participant's left, Y), and vertical (opposite to gravity, Z) directions were examined to determine if the forces in the stance phase of a turn differ from those produced in straight path walking. Average (horizontal) progression velocities were calculated from the movement of the heel, lateral malleolus, and tibial tuberosity markers; these velocities did not differ (all p's > 0.01). Consequently, the value of progression velocity calculated from the tibial tuberosity is used throughout this report.

Traditionally, the gait cycle is divided into stance and swing phases, which are identified by the first initial contact, when the swing foot comes in contact with the ground; toe-off (TO), when the toe of the stance foot loses contact with the ground; and the second initial contact, when the ipsilateral foot contacts the ground again. Stance is defined as initial contact to toe-off; swing is defined as toe-off to ipsilateral initial contact. In walking humans, initial contact in walking occurs through heel strike (HS), when the posterior heel of the foot touches the ground. Dividing the gait cycle into these phases allows specific gait events to be compared across multiple strides.

We used the force plates to determine when HS and TO occurred (Chang, Huang, Hamerski, & Kram, 2000); stance occurred when the vertical GRF exceeded 40N. We divided stance into two phases: braking and propulsion. In this study, braking was defined as the period

in the stance between when HS occurs and when the sole of the foot is in full contact (i.e., flat on the ground). Propulsion was defined as the period of time between when the heel begins to rise off the ground and TO. The vertical velocity of the first metatarsal head and the heel were calculated to determine when the foot is in full contact and when the heel starts to rise, respectively. All calculations were performed on each trial using a custom-developed MatLab code (Mathworks, Nantucket, MA).

Analysis

For both braking and propulsive phases, nine force components were selected as representative of each step: maximum forward force (MaxX), side force at MaxX, vertical force at MaxX, maximum side force (MaxY), forward force at MaxY, vertical force at MaxY, maximum vertical force (MaxZ), forward force at MaxZ, and side force at MaxZ. A summary of all the forces are provided in the supplemental material.

The differences between force plates C and A in the maximum GRF components were calculated for the braking and propulsion stage of a stride. A variable was generated to indicate whether a trial included a turn or was in a straight path (0=straight path, 1=turn). Using an analysis of variance (ANOVA) with correction for repeated measures, we determined whether or not these differences associated with the turning condition were the same as those while walking in a straight path. GRF components were also normalized to control for variation in the participant's body mass; however, the analysis of the normalized forces did not produce different results from those using the raw GRF components. All statistical analyses were performed in Stata (StataCorp, College Station, TX) with $\alpha=0.05$.

Results

Maximum Forward Forces

During braking, the maximum forward forces differ between straight and turning conditions ($p<0.001$). Both side ($p<0.001$) and vertical ($p<0.001$) forces that occur at MaxX are also different [Table 3 Fig. 2]. Maximum forward forces ($p<0.001$) and side forces ($p<0.001$) at MaxX forces in propulsion also differ between straight and turning conditions. Vertical forces at MaxX do not display a significant difference between conditions ($p=0.10$) [Table 4].

Maximum Side Forces

Maximum side forces also differ between straight and turning conditions during braking ($p<0.001$) and propulsion ($p<0.001$). Forward ($p<0.001$) and side ($p<0.001$) forces at MaxY are also different [Table 3; Fig. 3] in braking. In propulsion, forward forces are different ($p<0.001$) while vertical forces are not different ($p=0.12$) at MaxY [Table 4 Fig. 4].

Maximum Vertical Forces

In both stance phases**,** the magnitude of the maximum vertical force is not different between conditions ($p>0.05$) [Fig. 5], while the forward and side forces that occur at MaxZ are different (all p's <0.001) [Table 3 and 4].

Discussion

The results presented here demonstrate that the GRF components required to make a turn differ from those required to move in a straight path in both braking and propulsive phases of stance. During braking, the magnitude of both forward and side forces are higher in a turn than for walking in a straight path. As an individual turns, the body slows in its current course in order to initiate the directional change, which requires a force at an angle to the initial direction of travel and in the new direction of travel. Similarly, the propulsive phase also shows an increase

in the magnitude of forward forces of on average 230N, an increase of 150%. In turning, the side and forward forces are effectively "swapped" (Fig. 6). Importantly, not only are the magnitudes of the GRF components higher, but the side force, i.e., the force that redirects the body, is on average 207 N higher (an increase of 2491%), meaning that the resultant GRF on the foot that is braced for a turn has a different orientation. Given that the foot is asymmetric, analyses of the bones of the foot need to be reconsidered. For example, a side load applied to a metatarsal potentially produces a different osteological response (one due to bending stress, which is characterized by compressive and tensile regions) than does an axial compressive load (which creates uniform compression).

While walking, the stance foot transmits the GRF to the leg through the most direct path (Qingguo Wang et al., 2016). Both of these peak force events are different in turns, prompting the question of how this change of magnitude and direction affects the bones of the foot. Injury can occur when bones and soft tissue experience applied loads in directions that exceed their capabilities (Jin, 2014; Scott & Winter, 1990). While walking in a straight path is an important "design condition" for the foot, other events that occur with regularity are also important to consider. Changing direction while walking is such an event. Understanding how these forces translate into differences in the joint forces and moments of the foot is a logical next step.

Despite the consistent and significant results obtained, several characteristics of the study limit it. The force plates that were used to collect these data are positioned in a straight path relatively close to each to each other and this arrangement was not customizable. While we were able to collect force data from the step in which the change of direction occurs, as well as the two steps before the turn, we were unable to collect the forces generated from the step directly after a turn occurred.

Conclusion

The GRF components that are required to change the direction of travel are different than those produced to walk in a straight path. Although vertical forces of a turn are not different from those produced from walking in a straight line, the forward and side forces are higher during a turn than during walking in a straight line. Additional work is ongoing to understand how these differences affect joint forces and moments of the foot and ankle.

Chapter 4: Appendix

Chapter 4: References

Aiello, L., & Dean, C. (2002). *An Introduction to Human Evolutionary Anatomy* (1st ed.). Academic Press.

Bassett, D. R., Schneider, P. L., & Huntington, G. E. (2004). Physical Activity in an Old Order Amish Community. *Medicine & Science in Sports & Exercise*, *36*(1), 79–85. https://doi.org/10.1249/01.MSS.0000106184.71258.32

Bassett, D. R., Wyatt, H. R., Thompson, H., Peters, J. C., & Hill, J. O. (2010). Pedometer-Measured Physical Activity and Health Behaviors in U.S. Adults. *Medicine & Science in Sports & Exercise*, *42*(10), 1819–1825. https://doi.org/10.1249/MSS.0b013e3181dc2e54

Bischof, J. E., Abbey, A. N., Chuckpaiwong, B., Nunley, J. A., & Queen, R. M. (n.d.). Three-dimensional ankle kinematics and kinetics during running in women. *Gait Posture*, *31*(4), 502–505. https://doi.org/S0966-6362(10)00063-9 [pii]10.1016/j.gaitpost.2010.02.010

Bowden, R. E. (1967). The functional anatomy of the foot. *Physiotherapy*, *53*(4), 120–126.

Cavagna, G. A., Thys, H., & Zamboni, A. (1976). The sources of external work in level walking and running. *The Journal of Physiology*, *262*(3), 639–657. https://doi.org/10.1113/jphysiol.1976.sp011613

Cavanagh, P. R., & Lafortune, M. A. (1980). Ground reaction forces in distance running. *Journal of Biomechanics*, *13*(5), 397–406. https://doi.org/10.1016/0021-9290(80)90033-0

Chang, Y. H., Huang, H. W., Hamerski, C. M., & Kram, R. (2000). The independent effects of gravity and inertia on running mechanics. *The Journal of Experimental Biology*, *203*(Pt 2), 229.

Chehab, F. F., Pontzer, H., Raichlen, D. A., Wood, B. M., Mabulla, A. Z. P., Racette, S. B., & Marlowe, F. W. (2012). Hunter-Gatherer Energetics and Human Obesity. *PLoS ONE*, *7*(7), e40503. https://doi.org/10.1371/journal.pone.0040503

Frost, H. M. (1982). Mechanical determinants of bone modeling. *Metabolic Bone Disease & Related Research*, *4*(4), 217.

Hader, K., Palazzi, D., & Buchheit, M. (2015). Change of direction speed in soccer: how much braking is enough?(Original scientific paper). *Kinesiology*, *47*(1), 67.

Huang, T.-W. P., & Kuo, A. D. (2014). Mechanics and energetics of load carriage during human

walking. *The Journal of Experimental Biology*, *217*(Pt 4), 605. https://doi.org/10.1242/jeb.091587

Jin, J. (2014). Running Injuries. *JAMA*, *312*(2), 202. https://doi.org/10.1001/jama.2013.283011

Marlowe, F. W. (2005). Hunter-gatherers and human evolution. *Evolutionary Anthropology: Issues, News, and Reviews*, *14*(2), 54–67. https://doi.org/10.1002/evan.20046

Minetti, A. E. (1995). Optimum gradient of mountain paths. *Journal of Applied Physiology*, *79*(5), 1698–1703. https://doi.org/10.1152/jappl.1995.79.5.1698

Morio, C., Lake, M. J., Gueguen, N., Rao, G., & Baly, L. (2009). The influence of footwear on foot motion during walking and running. *Journal of Biomechanics*, *42*(13), 2081–2088. https://doi.org/10.1016/J.JBIOMECH.2009.06.015

Morris, J. M. (1977). Biomechanics of the foot and ankle. *Clinical Orthopaedics and Related Research*, (122), 10–17.

Nilsson, J., & Thorstensson, A. (1989). Ground reaction forces at different speeds of human walking and running. *Acta Physiologica Scandinavica*, *136*(2), 217–227. https://doi.org/10.1111/j.1748-1716.1989.tb08655.x

Orien, W. P., Weed, J. H., & Root, M. L. (1977). *Normal and abnormal function of the foot*. (W. P. Orien & J. H. Weed, Eds.) (1st ed.). Los Angeles: Los Angeles : Clinical Biomechanics Corp.

Rue, M. J., & Kramer, P. A. (2017). Minimal energetic expenditure of women walking burdened on gradients in urban environments. *American Journal of Human Biology*, *29*(1), n/a-n/a. https://doi.org/10.1002/ajhb.22907

Ruff, C., Holt, B., & Trinkaus, E. (2006). Who's afraid of the big bad Wolff?: "Wolff's law" and bone functional adaptation. *American Journal of Physical Anthropology*, *129*(4), 484–498. https://doi.org/10.1002/ajpa.20371

Scott, S. H., & Winter, D. A. (1990). Internal forces of chronic running injury sites. *Medicine and Science in Sports and Exercise*, *22*(3), 357.

Stokes, I. A., Hutton, W. C., & Stott, J. R. (1979). Forces acting on the metatarsals during normal walking. *J Anat*, *129*(Pt 3), 579–590.

Voloshina, A. S., Kuo, A. D., Daley, M. A., & Ferris, D. P. (2013). Biomechanics and energetics of walking on uneven terrain. *Journal of Experimental Biology*, *216*(21), 3963–3970. https://doi.org/10.1242/jeb.081711

Wang, Q., Pejhan, K., Wu, C. Q., & Telichev, I. (2016). Load Transfer Index for Composite Materials. *Volume 9: Mechanics of Solids, Structures and Fluids*, V009T12A009. https://doi.org/10.1115/imece2015-51176

Wilson, A. M., Hubel, T. Y., Wilshin, S. D., Lowe, J. C., Lorenc, M., Dewhirst, O. P., … West, T. G. (2018). Biomechanics of predator–prey arms race in lion, zebra, cheetah and impala. *Nature*, *554*(7691), 183–188. https://doi.org/10.1038/nature25479

Chapter 4: List of Tables

Participant	Sex	Age	Mass (kg)	Stature (cm)	Average Velocity of Straight Trial (m/s)	Average Velocity of Turning Trial (m/s)
1	F	20	57.6	163	1.4	1.3
2	M	29	88.9	180	1.3	1.3
3	F	28	66.4	162	1.3	1.2
4	M	42	87.3	172	1	1.1
5	F	55	82.3	168.5	1.2	1.2
6	F	19	54	162.5	1.3	1.2
7	F	26	86.2	170.2	1.1	1
8	F	28	90.5	175	1.2	1.2
9	F	29	63.6	171.5	1.1	1.2
10	M	29	120	187	1.2	1.1
11	M	28	90.7	180	1.3	1.2
12	M	43	84.8	173	1.2	1.1
13	M	45	63.3	170.2	1.3	1.3
14	M	22	78.2	180	1.2	1.2
15	M	21	78	183	1.1	1.2
16	F	21	69	172	1.1	1.1
17	M	36	74.3	172	1.1	1.2
18	F	22	98.5	167.5	1.2	1.2
19	M	34	89.2	182.4	1.2	1.2
20	M	29	86.5	177.8	1.2	1.2

Table 1: Anthropometrics of all participants.

	Definition

Anatomical Landmarks	
Heel	The location on the skin over the location where the Achilles tendon attaches to the calcaneus.
Dorsal Navicular	The location on the skin over the dorsal most prominent point of the navicular.
Navicular Tubercle	The location on the skin over the most prominent point of the navicular tubercle.
Head of the First Metatarsal	The location on the skin over the center of the head of the 1st metatarsal.
Base of the First Metatarsal	The location on the skin over the center of the base of the 1st metatarsal.
Head of the Fifth Metatarsal	The location on the skin over the center of the head of the 5st metatarsal.
Styloid process of the fifth metatarsal	The location on the skin over the most prominent point of the Styloid process of the fifth metatarsal.
Fat Pad	The location on the skin over the lateral surface of the calcaneus superior to the fat pad.
Lateral malleolus	The location on the skin over the most prominent point of lateral malleolus.
Medial malleolus	The location on the skin over the most prominent point of medial malleolus.
Tibial tuberosity	The location on the skin over the most prominent point of tibial tuberosity.
Medial tibial plateau	The location on the skin over the most prominent point of medial tibial plateau.
Lateral tibial plateau	The location on the skin over the most prominent point of lateral tibial plateau.

Table 2: Location and definition of the anatomical landmarks of the foot, ankle, and calf.

	Average Difference in forces (N) between force plates																				
	X								Y							Z					
	A0-C0 (N)	A1-C1 (N)	MD (N)	SE	95% CI	R^2	P	A0-C0 (N)	A1-C1 (N)	MD (N)	SE	95% CI	R^2	P	A0-C0 (N)	A1-C1 (N)	MD (N)	SE	95% CI	R^2	P
Max X	10.71	-41.88	-52.59	4.13	(-61.23) - (-43.95)	0.65	<0.001	-2.15	-78.55	-76.40	5.32	(-87.55) - (-65.26)	0.80	<0.001	15.28	-67.52	-82.80	15.63	(-115.53) - (-50.08)	0.33	<0.001
Max Y	1.23	-48.41	-49.64	9.18	(-68.86) - (-30.42)	0.77	<0.001	-0.67	-89.81	-89.14	5.54	(-100.73) - (-77.56)	0.76	<0.001	4.93	-71.94	-76.87	37.85	(-156.08) - 2.36	0.04	0.06
Max Z	12.25	-55.30	-67.55	4.49	(-76.95) - (-58.15)	0.70	<0.001	-1.63	-79.98	-78.34	4.94	(-88.69) - (-68.00)	0.81	<0.001	2.43	-23.10	-25.52	0.51	(47.52) - (-3.53)	0.09	0.03

	Average Difference in normalized forces between force plates																				
	X								Y							Z					
	A0-C0	A1-C1	MD	SE	95% CI	R^2	P	A0-C0	A1-C1	MD	SE	95% CI	R^2	P	A0-C0	A1-C1	MD	SE	95% CI	R^2	P
Max X	0.013	-0.055	-0.068	0.567	(-0.080) - (-0.056)	0.63	<0.001	-0.003	-0.101	-0.098	0.007	(-0.112) - (-0.083)	0.79	<0.001	0.018	-0.087	-0.105	0.019	(-0.145) - (-0.065)	0.34	<0.001
Max Y	0.002	-0.063	-0.066	0.012	(-0.091) - (-0.040)	0.35	<0.001	-0.002	-0.114	-0.112	0.006	(-0.124) - (-0.101)	0.79	<0.001	0.010	-0.086	-0.096	0.049	(-0.199) - (.007)	0.05	0.07
Max Z	0.015	-0.072	-0.087	0.006	(-0.099) - (-0.074)	0.69	<0.001	-0.0023	-0.102	-0.100	0.006	(-0.112) - (-0.087)	0.81	<0.001	0.003	-0.030	-0.033	0.013	(-0.060)- (-0.005)	0.09	0.02

Table 3: Mean ground reaction forces between walking in a straight path and a 90° turn during the braking phase. Forces are presented in newtons as well as normalized for individual's weight.

	Average Difference in forces (N) between force plates																			
	X							Y							Z					
	A0-C0 (N)	A1-C1 (N)	MD (N)	SE	95% CI	R^2	P	A0-C0 (N)	A1-C1 (N)	MD (N)	SE	95% CI	R^2	P	A0-C0 (N)	A1-C1 (N)	MD (N)	SE	95% CI	R^2	P
Max X	2.18	-232.52	-234.70	11.79	(-259.383) - (-210.01)	0.91	<0.001	-3.58	-89.57	-85.99	6.57	(-99.74) - (-72.23)	0.76	<0.001	0.77	-16.53	-17.31	14.88	(-48.4605) - 13.85	0.02	0.26
Max Y	17.50	-95.47	-112.98	10.28	(-134.49) - (-91.47)	0.60	<0.001	-3.62	-179.22	-175.60	8.19	(-192.7531) - (-158.45)	0.90	<0.001	-25.46	-4.76	20.70	17.03	(-14.94763) - 56.35	0.01	0.24
Max Z	2.30	-134.75	-137.05	8.08	(-153.95) - (-120.15)	0.84	<0.001	-3.58	-166.20	-162.63	7.87	9-179.10) - (-146.15)	0.89	<0.001	0.35	3.52	3.17	11.24	(-20.36) - 26.69	0.001	0.78

	Average Difference in normalized forces between force plates																			
	X							Y							Z					
	A0-C0	A1-C1	MD	SE	95% CI	R^2	P	A0-C0	A1-C1	MD	SE	95% CI	R^2	P	A0-C0	A1-C1	MD	SE	95% CI	R^2	P
Max X	0.002	-0.292	-0.294	0.009	(-0.312) - (-0.275)	0.95	<0.001	-0.005	-0.113	-0.108	0.007	(-0.123) - (-0.094)	0.77	<0.001	0.001	-0.017	-0.018	0.017	(-0.054) - .019	0.02	0.33
Max Y	0.024	-0.122	-0.146	0.015	(-0.177) - (-0.116)	0.59	<0.001	-0.005	-0.227	-0.222	0.007	(-0.238) - (-0.207)	0.93	<0.001	-0.033	-0.007	0.026	0.020	(-0.016) - .068	0.01	0.21
Max Z	0.0021	-0.170	-0.172	0.008	(-0.189) - (-0.155)	0.86	<0.001	-0.005	-0.211	-0.206	0.008	(-0.222) - (-0.190)	0.90	<0.001	0.000	0.004	0.004	0.014	(-0.025) - (.033)	0.00	0.77

Table 4: Mean ground reaction forces between walking in a straight path and a 90° turn during the propulsion phase. Forces are presented in newtons as well as normalized for individual's weight.

Chapter 4: List of Figures

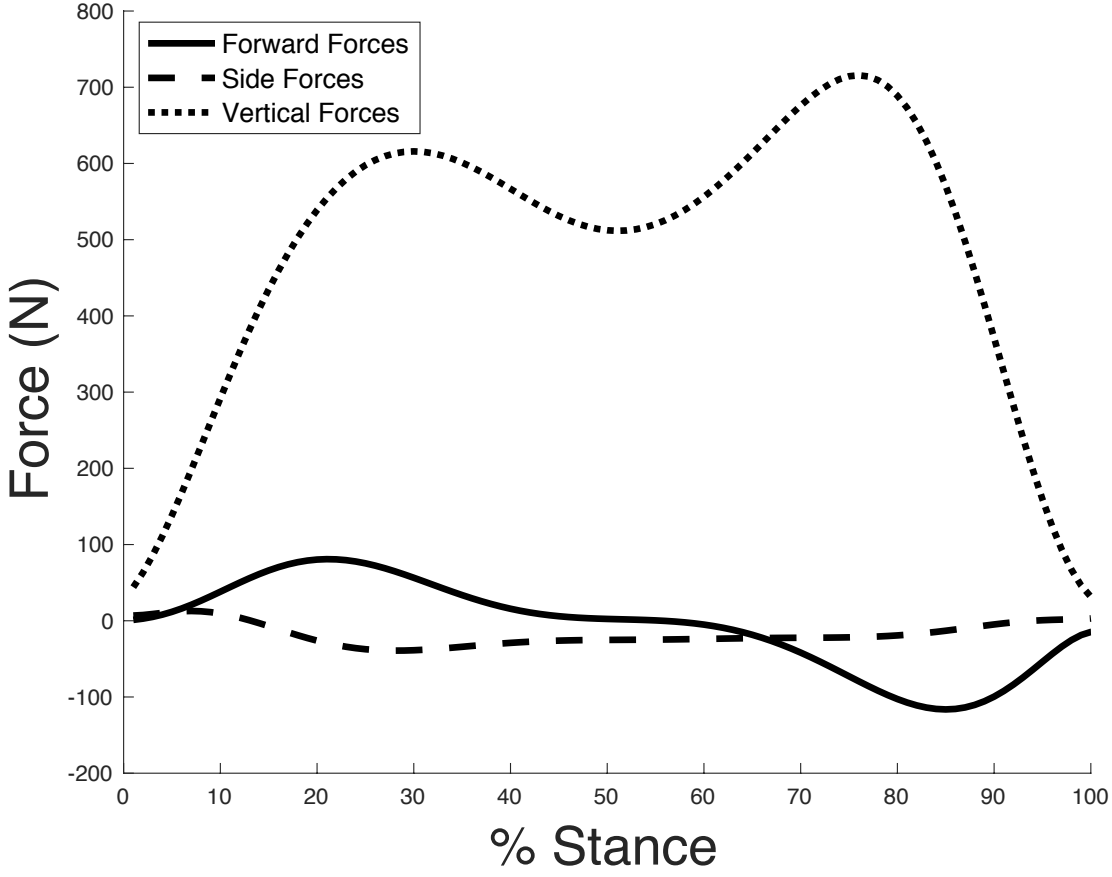

Figure 1: Forward (X; solid line), side (Y; dashed line), and vertical (Z; dotted line) forces from a single for a straight walking trial.

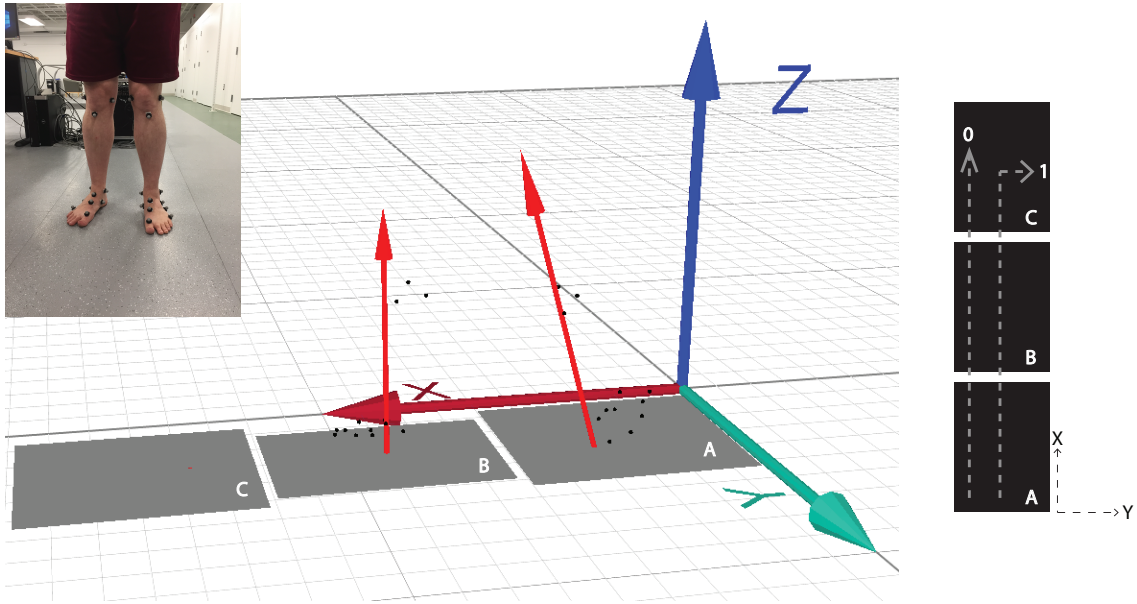

Figure 2: Participant with markers (a) and the virtual representation of the participant during a walking trial (b). Force plates are labeled A, B and C. A diagram of the walking protocol is depicted. The dotted lines represent the direction in which participants, 0 for a straight walking path and 1 for a 90° turn (c). The turn occurs on force plate C.

A)

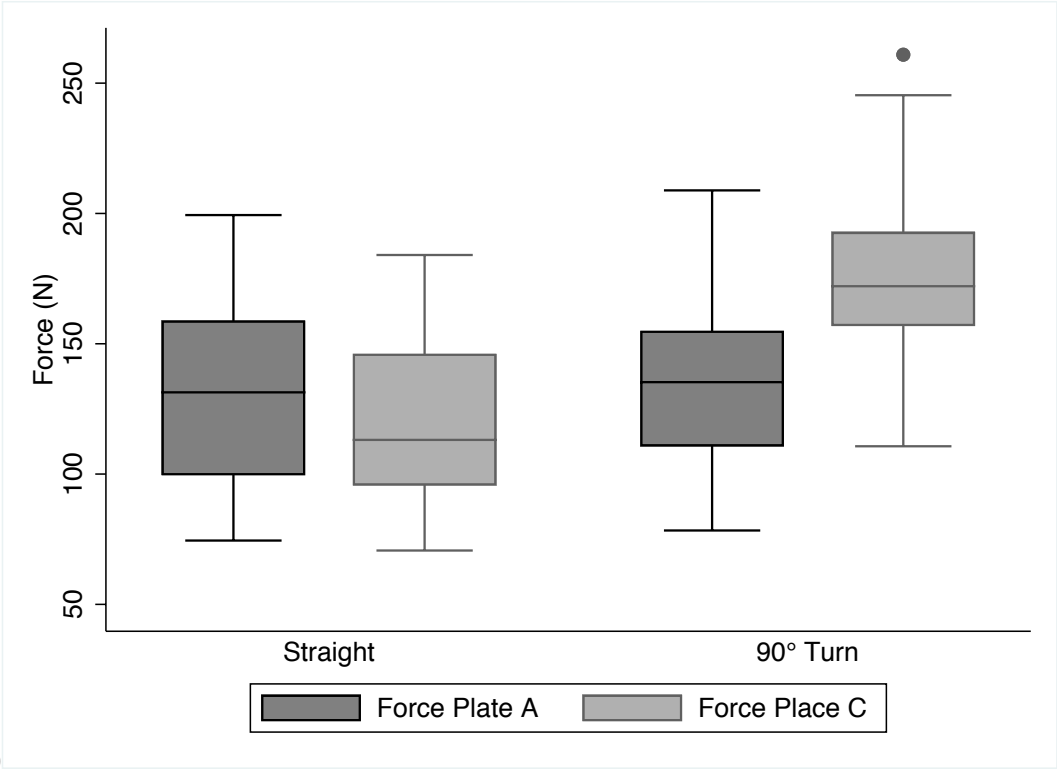
Force (N)
50
100
150
200
250
Straight
90° Turn
Force Plate A
Force Place C

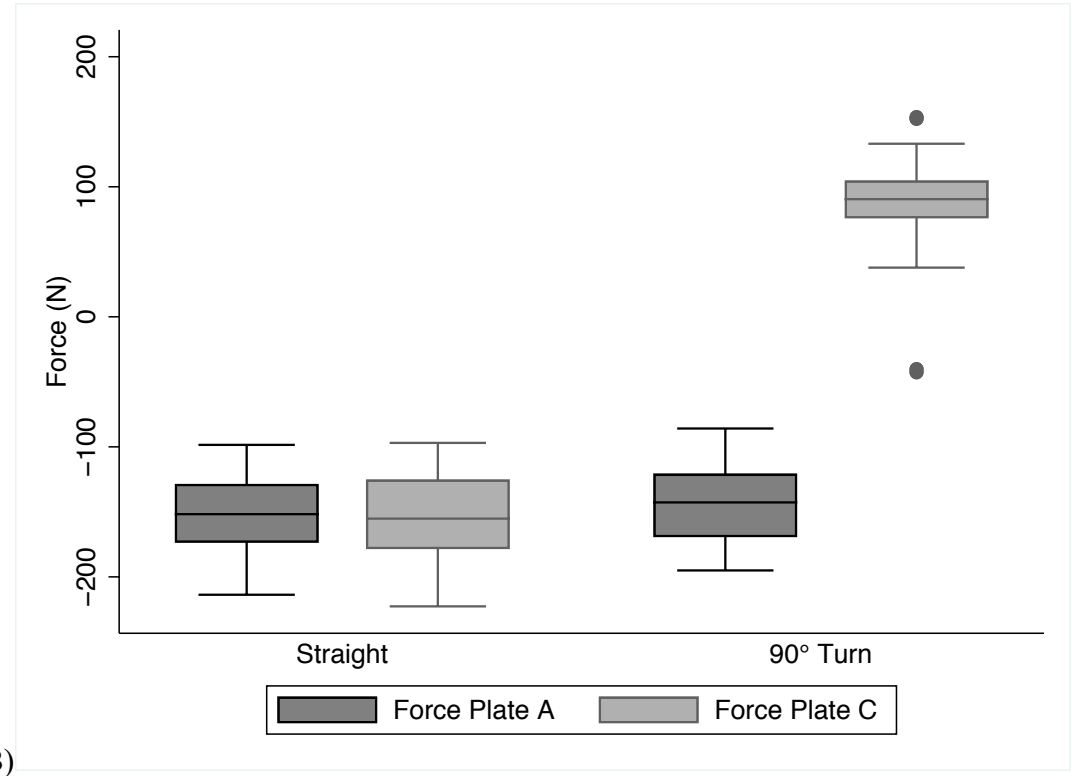

B)

Figure 3: Maximum forward (X) forces for force plate A and C for each walking condition for braking (A) and Propulsion (B).

A)

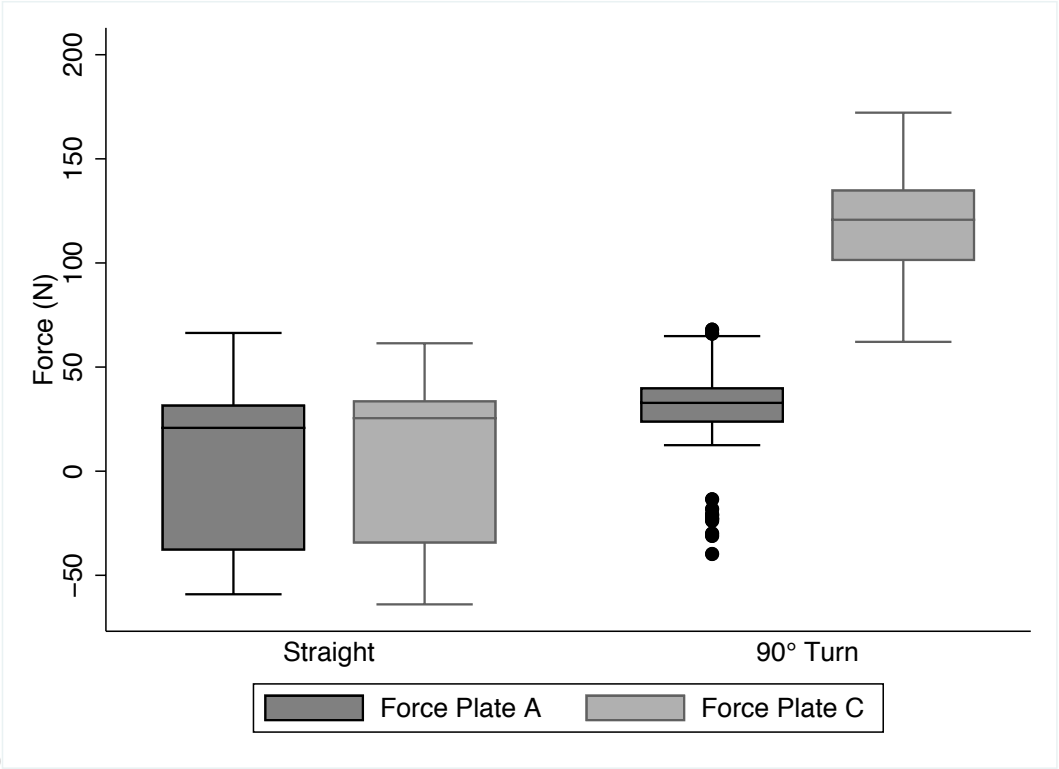
Force (N)
200
150
100
50
0
−50
Straight
90° Turn
Force Plate A
Force Plate C

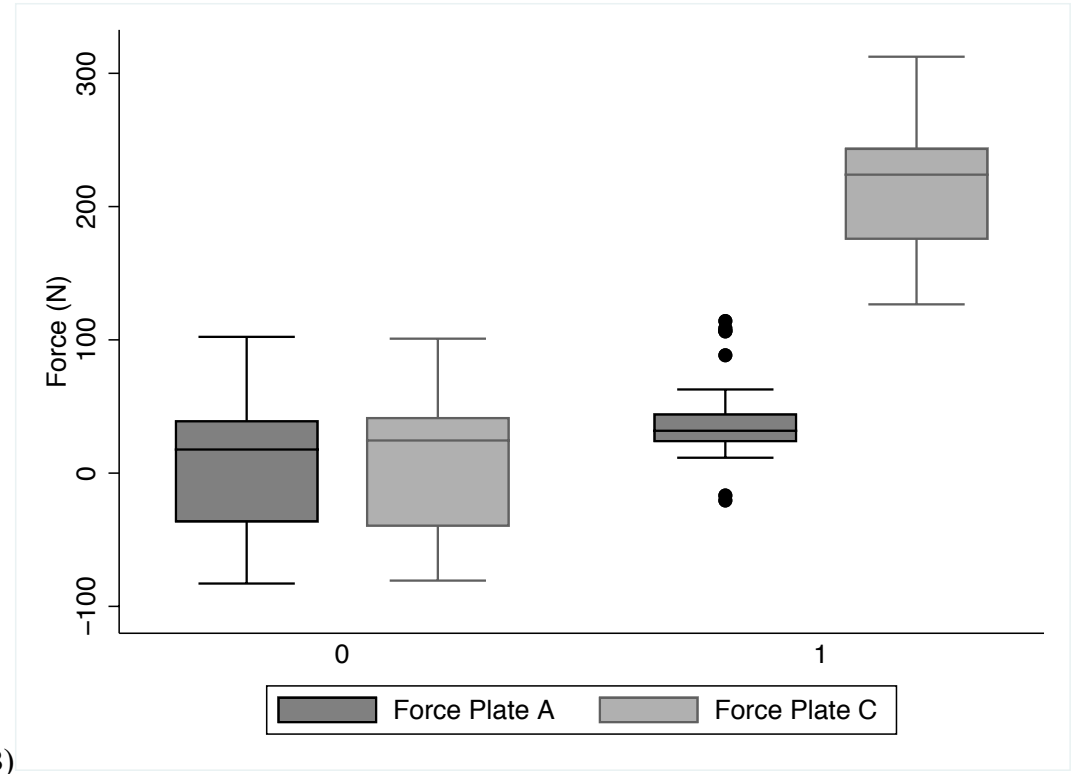

B)

Figure 4: Maximum side (Y) forces for force plate A and C for each walking condition for braking (A) and Propulsion (B).

A)

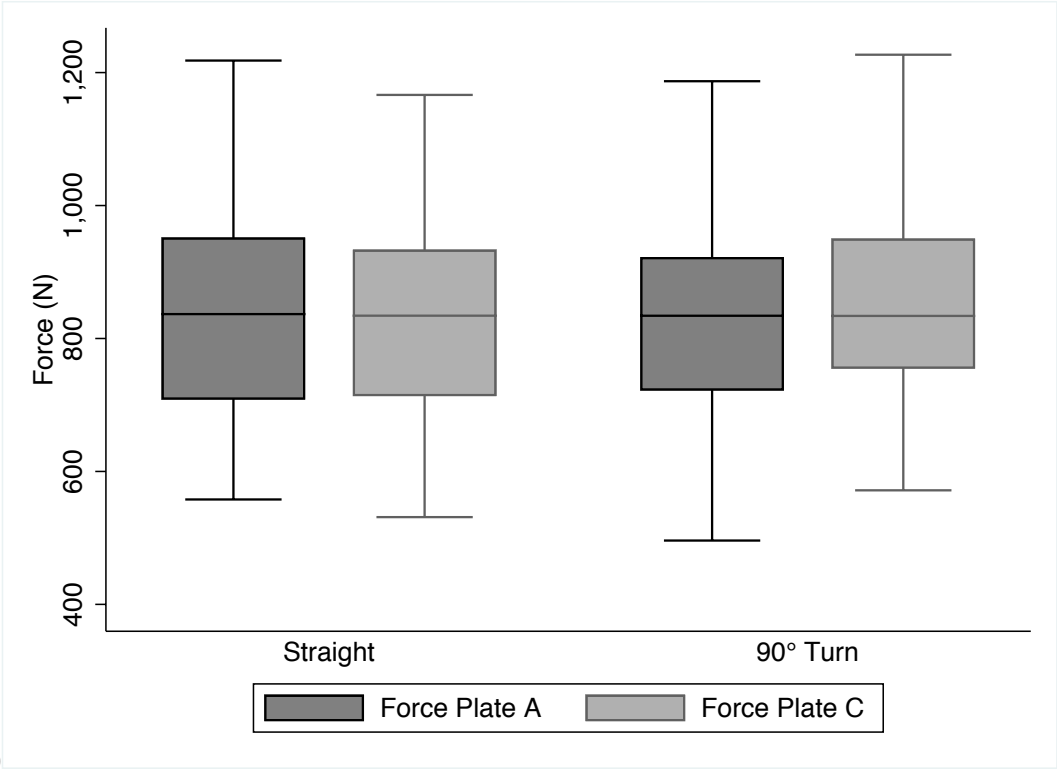
Force (N)
400
600
800
1,000
1,200
Straight
90° Turn
Force Plate A
Force Plate C

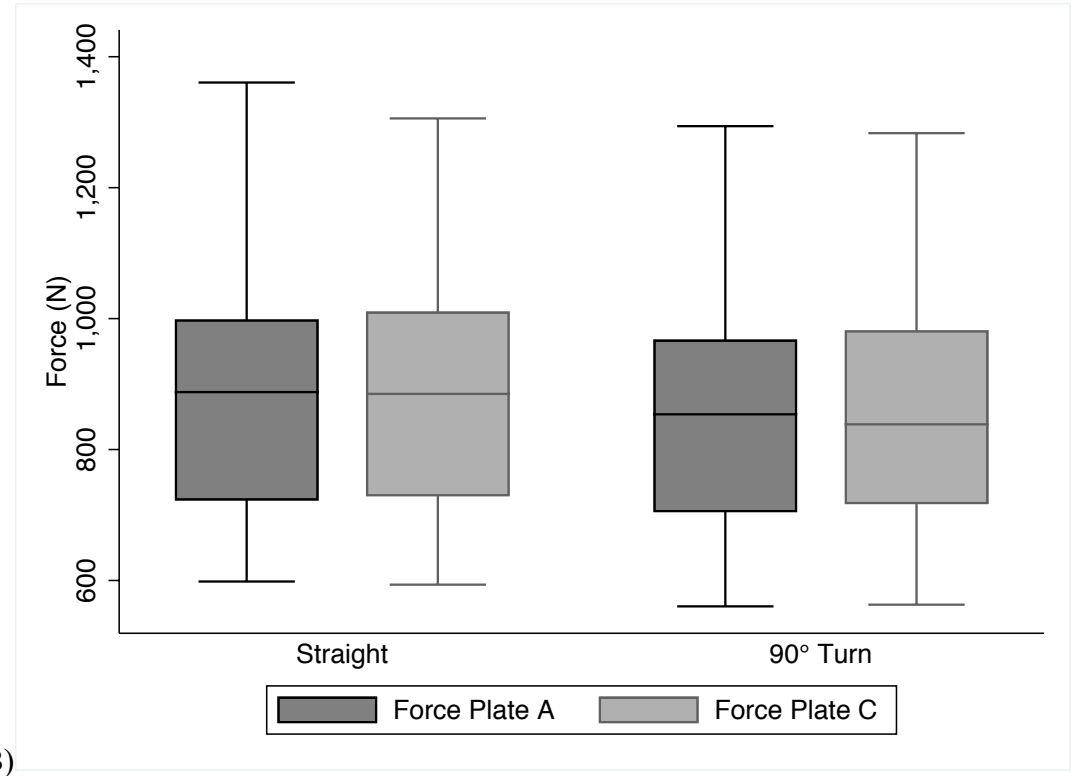

B)

Figure 5: Maximum vertical (Z) forces for force plate A and C for each walking condition for braking (A) and Propulsion (B).

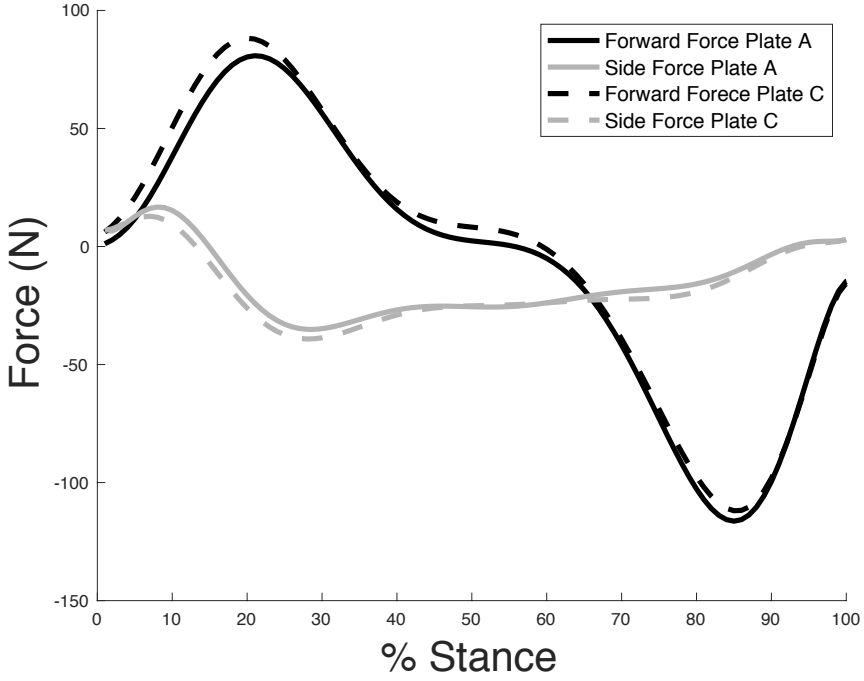
Forward Force Plate A
Side Force Plate A
Forward Forece Plate C
Side Force Plate C
Force (N)
% Stance
100
50
0
-50
-100
-150
0
10
20
30
40
50
60
70
80
90
100

(A)

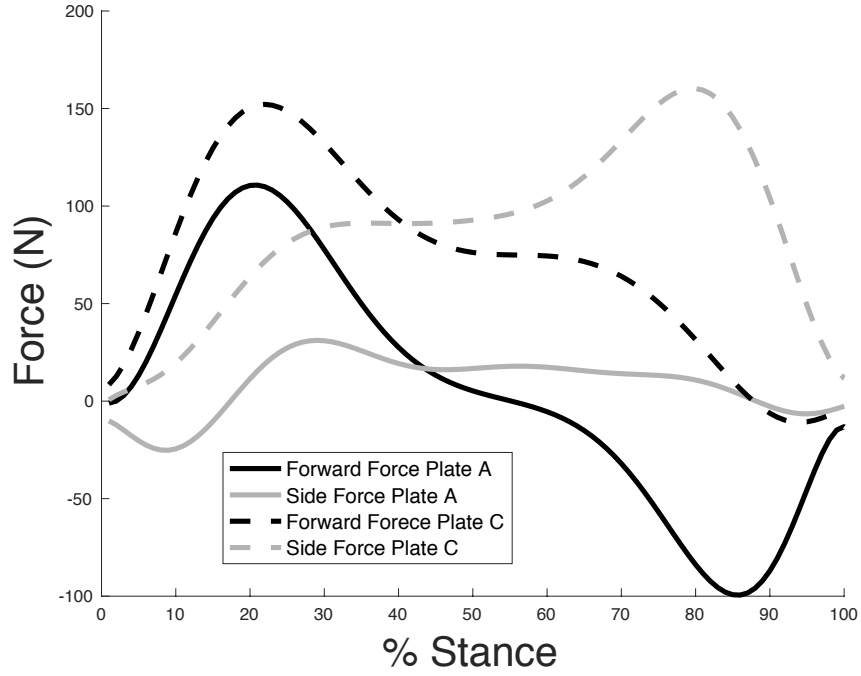

(B)

Figure 6: Forward (X) and Side (Y) forces for force plate A (solid line) and force plate C (dashed line) for a straight walking trial (A) and for a 90° turn (B).

Chapter 5: The influence of foot orientation on ground reaction force

Preface

The following chapter is a manuscript that will be submitted to Clinical Orthopaedics and Related Research in September 2019 authored by Steven G. Lautzenheiser, Adam D. Sylvester, and Patricia A. Kramer.

Introduction

Displaced fractures of the foot and ankle are often treated with open reduction and internal fixation. These fixation devices and how they are placed on the reduced fragments are designed to withstand typical loads experienced during bone healing. These fractures take considerable time to heal, necessitating a considerable post-surgical non-weightbearing period. After some amount of weightbearing commences, frequently the patient is instructed to limit their weightbearing to less than full body weight and in that time, the patient is first kept in a surgical boot, but then moves to a regular or rehabilitation shoe. Throughout this rehabilitation period, the goal is to provide sufficient stimulus to the bone to prevent bone loss while limiting the chance of re-injury. Both of these goals require understanding the forces applied to the foot in walking.

Most understanding of the forces to which bones of the foot are subjected is premised on data developed from force plates in laboratories that evaluate movement. These forces are classically described in terms of anatomical planes and directions, frequently with X and Y axes defining the horizontal plane, the X and Z axis defining the sagittal plane, and Y and Z axes the coronal plane

(Figure 1). This anatomical or world coordinate system (WCS) aligns well with both the physical surroundings of the laboratory and most skeletal elements and joints, such as the femur and hip. The foot, particularly during walking, does not, however, match to these primary axes. Most people angle their distal foot laterally (toe-out or external rotation of the foot) during walking.

The proximodistal and vertical forces are large in walking in a straight line at normal velocity, but the mediolateral forces are relatively low (Figure 3). This would lead one to believe that, for instance, side forces on the metatarsals would also be negligible. Due to external rotation, however, proximodistal forces produce both axial and bending loads in the metatarsals and other bones that are oriented longitudinally. The degree to which foot placement impacts the internal forces and moments of the foot and ankle remains unclear. Foot placement might create trivial variations from forces appreciated from a global perspective or foot placement might change internal forces substantially. Consequently, the purpose of this work is to determine if forces aligned in a foot coordinate system differ from those in the world coordinate system in order to inform orthopaedic treatment and rehabilitation.

Methods

Subject population

Twenty healthy participants (9 females, 11 males) were recruited for this study. Body mass (kg) and stature (cm) were measured for each participant (Table 1). To our knowledge all participants were free of lower-limb injuries. The University of Washington's Institutional Review Board approved all aspects of this study (IRB#: STUDY00001125).

Experimental Protocol

The experimental protocol used for this study was previously reported in (reference to paper 2 goes here). Using their self-selected normal pace, participants walked unshod the length of the gait lab in a straight path. Ten infrared-reflective markers (5mm hemispherical markers) were affixed to the foot and ankle, including to the: first and fifth metatarsal heads, most dorsal portion of the foot superior to the navicular, navicular tubercle, styloid process of fifth metatarsal, base of the first metatarsal, the lateral surface of the calcaneus superior to the fat pad, the heel (insertion of Achilles tendon to calcaneus), the lateral malleolus, and the medial malleolus. Each participant's kinetic and kinematic data were measured using a four-force plate (Kistler, Switzerland) and 10-camera motion capture system (Qualisys, Sweden) in the Amplifying Movement & Performance laboratory (AMP) of the University of Washington. Marker data and GRFs from each force plate were collected at 120 Hz (i.e., the time between frames is 1/120 seconds) and the raw marker data were filtered at 10 Hz with a 4^{th} order, low pass zero-lag Butterworth filter.

The foot coordinate system

The marker and GRF data are collected in the "world" (or laboratory) coordinate system (WCS), a three-dimensional Cartesian coordinate system (i.e., one where the location of any point is defined by reference to an origin with three lengths (coordinates)), that aligns with the physical space (floor and walls) of the laboratory. The origin of the WCS is the corner of a force plate (known as force plate A). The WX axis is in the (typical) direction of progression while the WY axis is to the side. The WZ axis is vertical (i.e., aligned with gravity). The individual moves through this space, producing GRFs and marker trajectories that are recorded.

The foot coordinate system (FCS) is another Cartesian coordinate system, one that moves with the foot as the foot moves through the laboratory. The FCS was established in order to examine forces on the elements of the foot (e.g. bones, tendons) because the internal forces of the elements need to be understood relative to their orientation and without regard to where the foot is in the laboratory.

Definition of key variables

The gait cycle is divided into a stance and a swing phase. The stance phase is the period between when the foot makes initial contact with the ground and when the toe lifts off the ground. The swing phase occurs between toe-off and ipsilateral initial contact. Dividing the gait cycle into these phases allows specific gait events to be compared across multiple strides. During stance, the foot supports the body and the force plate registers forces in the WCS. We divided stance into two equal phases: the first and last 50%. WX and WZ forces exhibit two peaks (Figure with WCS forces) so this approach was taken in order to capture the maximum GRF produced when the foot makes initial contact with the ground (a period of time when the stance limb is slowing the body (braking)) and when the foot pushes off the ground (when the stance limb accelerates the body (propulsion)).

Which foot (left or right) that was in contact with force plate A for each trial was determined using the location of the heel markers and the known location of force place A. Trial side is defined by the foot side that produces the GRF. All left foot and ankle markers were reflected about the world X axis in order to create (pseudo-) right feet. The origin (0,0,0) of the FCS was set to the heel marker and all frames of the marker positions and forces were translated so that the heel marker was positioned at the origin and then

were rotated such that the long axis of the foot (Figure 3) a line created between the heel marker and the midpoint between 1st metatarsal and 5th metatarsal markers, was aligned with the foot X-axis. In the foot coordinate system, X is proximodistal, Y is mediolateral, and Z is superoinferior (Figure 4).

Force data from plate A was analyzed for this study. The individual components of the GRFs were examined to determine if the forces in the FCS differ from those WCS. All calculations were performed using a custom-developed MatLab code (Mathworks, Nantucket, MA).

Analysis

For both periods of the stance phase, nine force components in both WCS and FCS were extracted as representative of each step: maximum X-force (maxX), Y-force at maxX, Z-force at maxX, maximum Y-force (maxY), X-force at maxY, Z-force at maxY, maximum Z-force (maxZ), X-force at maxZ, and Y-force at maxZ. The differences between the WCS and the FCS maximum GRFs were calculated. Linear regression with correction for repeated measures was used to determine whether or not the forces in the FCS are different that those in the WCS. All statistical analyses were performed in Stata (StataCorp, College Station, TX) with $\alpha = 0.05$.

Results

The transformation into the FCS from the WCS should not change the magnitude of the GRF in any frame. Consequently, GRFs in the both the WCS and the FCS were compared using a student's t-test to confirm that the transformation did not change the GRFs magnitude ($p<0.001$, Figure 5).

In both early and late stance, maximum mediolateral forces are greater in the FCS than WCS. The increase in side forces in the FCS averages between 150-200 N, with some individuals exhibiting increases of greater than 350 N. The direction of the force also changes. In WCS the maximum force is directed toward the centerline, while in FCS it is lateral. Since the GRF magnitude does not change, this increase in side forces is due to decreases in the other two components. In both early stance, Z forces are relatively unchanged but in late stance FZ is somewhat less than WZ. Maximum WX is higher in magnitude than FX in early stance but not in late stance (Tables 1-2; Figure 6-8).

Discussion

As anticipated, projecting the GRF into FCS produces a different picture of internal forces than is typically understood from WCS. The long axis of the foot is angled to the direction of progression which transforms the braking and propulsive forces (WX) into axial (FX) and bending (FY) forces in the foot.

Injuries that are sensitive to these mediolateral forces include metatarsal fractures, Lisfranc injuries, talar neck fractures, and distal fibular fractures, among others. Implants used to stabilize fractures after reduction with internal fixation need to be designed to withstand these forces. For instance, foot side forces are transferred from the talus to the medial or lateral malleolus (depending on the direction of the force). If the force is laterally oriented, the talus pushes into the distal fibula, which is cantilevered and is supported against these forces by the interosseous membrane. Fibular fractures can be reinforced by a plate along the length of the fibula with or without syndesmotic screws. Plates are not strong in bending about their thickness, but the syndesmotic screw provides a constraint to

reinforce the fibula. With substantial lateral force a likely occurrence once normal gait commences, internal fixation should be developed to accommodate the applied forces.

In addition to considering implant choice and placement, the return to walking during the rehabilitation period might be modified to preclude toe-out or require limited heelstrike or toe-off for an extended period. Little information exists to inform the biomechanics of walking in a post-injury boot (), but if the foot turns out in boot-walking, then additional therapeutic instructions might be warranted.

Chapter 5: Appendix

Chapter 5: List of Tables

Table 1: Mean differences for both periods of the stance phase. for negative values indicate that the magnitude is larger.

	First 50% of stance								
	X			Y			Z		
	Mean difference (N)	Minimum (N)	Maximum (N)	Mean difference (N)	Minimum (N)	Maximum (N)	Mean difference (N)	Minimum (N)	Maximum (N)
Max X	127.46	-21.38	356.32	-153.78	-250.85	-60.07	162.83	-45.67	492.07
Max Y	33.68	-77.98	179.01	-201.80	-360.28	-100.94	128.13	-455.47	398.24
Max Z	90.17	-8.41	200.45	-173.55	-298.61	-76.20	6.14	-6.09	44.39

	Last 50% of stance								
	X			Y			Z		
	Mean difference (N)	Minimum (N)	Maximum (N)	Mean difference (N)	Minimum (N)	Maximum (N)	Mean difference (N)	Minimum (N)	Maximum (N)
Max X	-306.02	179.76	567.89	-131.78	-223.59	-76.14	145.58	70.30	258.76
Max Y	-280.66	-50.27	670.90	-168.58	-292.28	-100.26	73.75	-393.58	484.08
Max Z	-193.36	84.46	362.64	-159.27	-272.60	-88.74	66.33	17.71	139.99

Table 1: Mean differences for both periods of the stance phase. for negative values indicate that the magnitude is larger.

Chapter 5: List of Figures

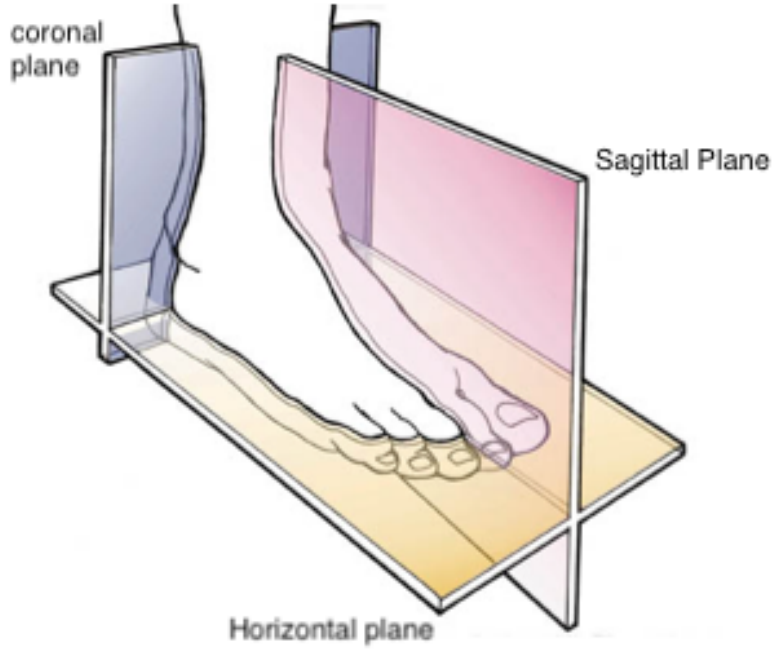

Figure 1: Anatomical planes on the human foot in the foot.

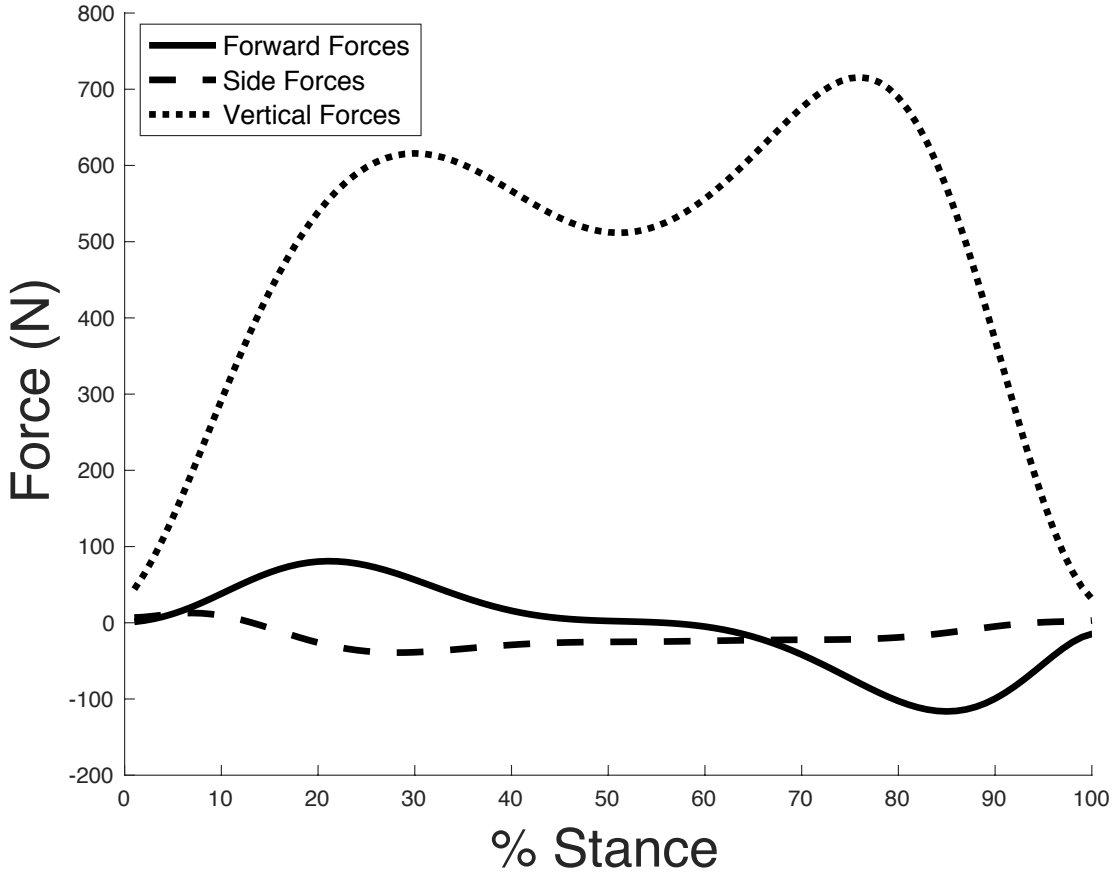

Figure 2: Typical Forward (X; solid line), side (Y; dashed line), and vertical (Z; dotted line) forces from a single walking trial.

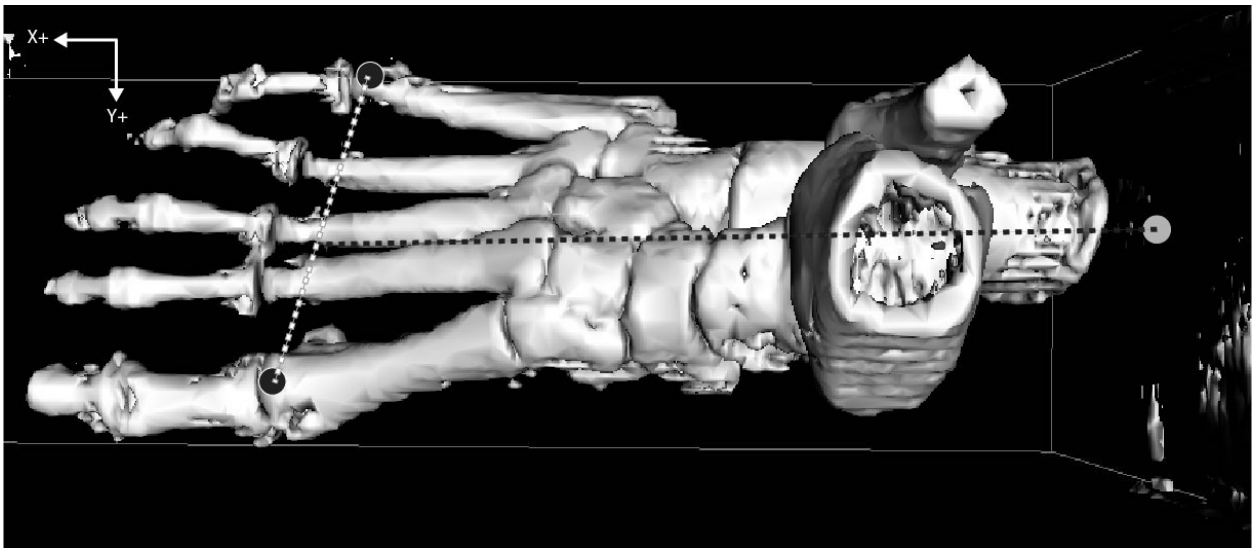

Figure 3: Virtual reconstruction of a foot The long axis of the foot (black dotted line) is created using the midpoint between markers for the 1st and 5th metatarsals and the heel. Markers in image are not to scale.

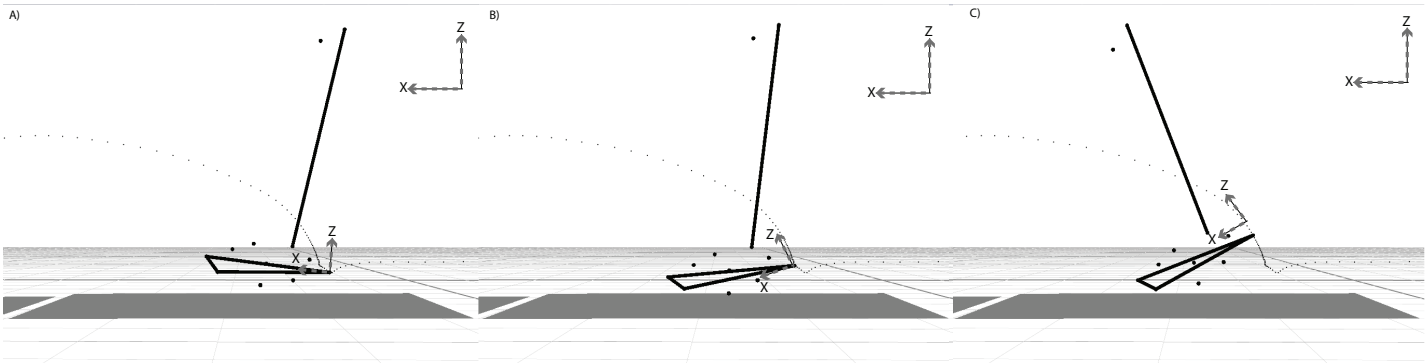

Figure 4: Comparison of the world coordinate system (WCS) and the foot coordinate system (FCS) at three stages of the gait cycle: (A) heel strike, (B) Midstance, and (C) Toe-off. The axis system for the WCS is in the corner of each frame while the axis for the FCS is near the heel.

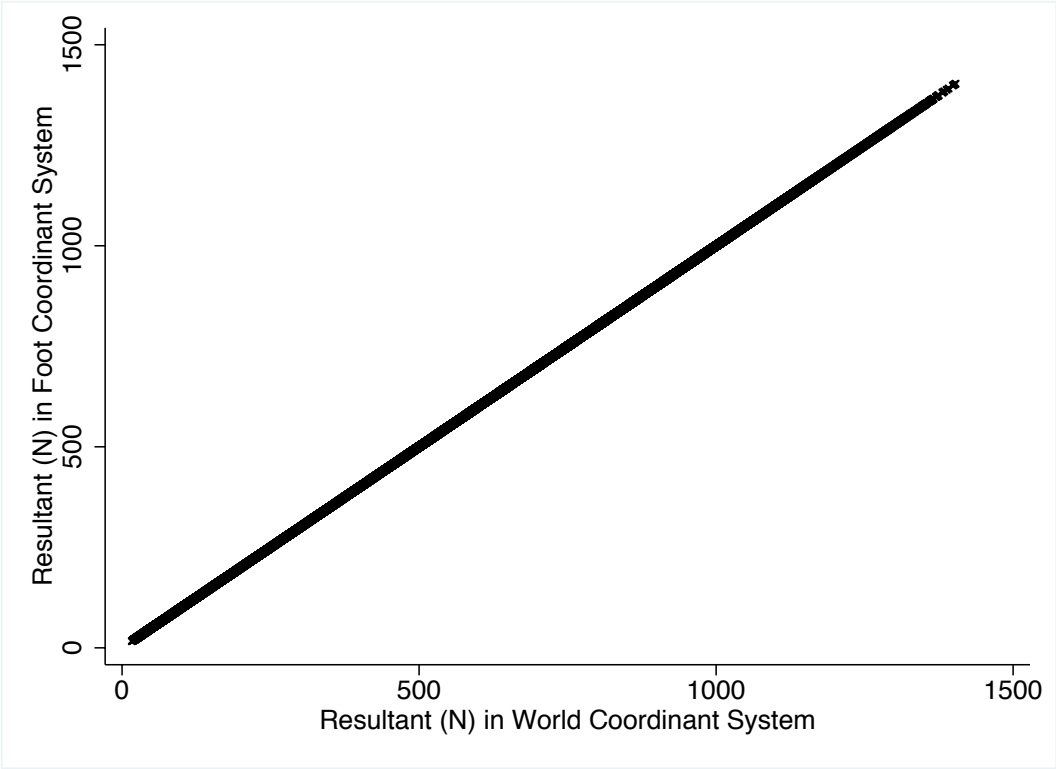

Figure 5: Resultants compared in both world coordinate system and foot coordinate system.

A)

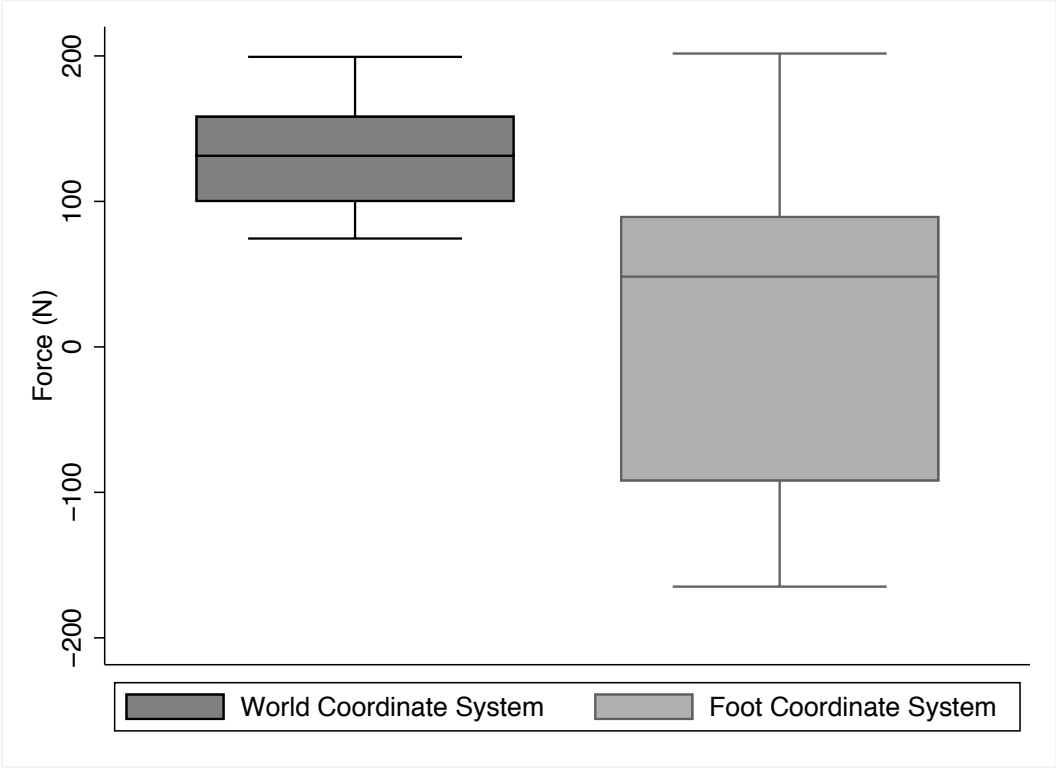

B)

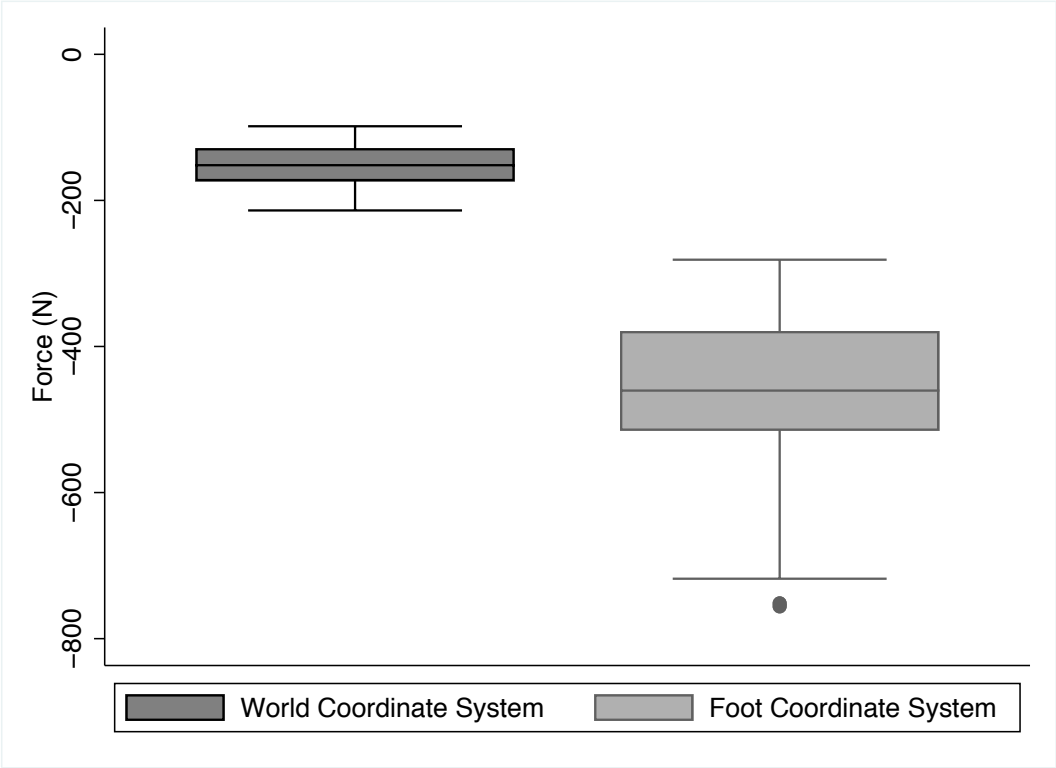

Figure 6: Maximum proximodistal (X) forces for early braking (A) and late (B) phase of the stance.

A)

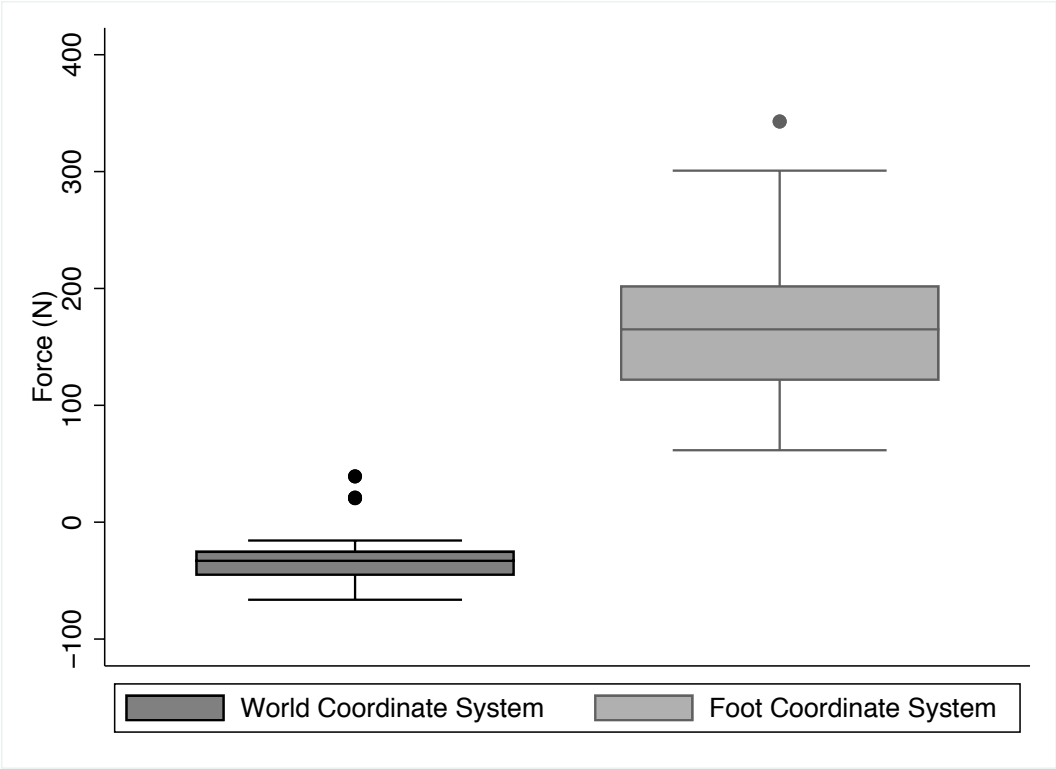

B)

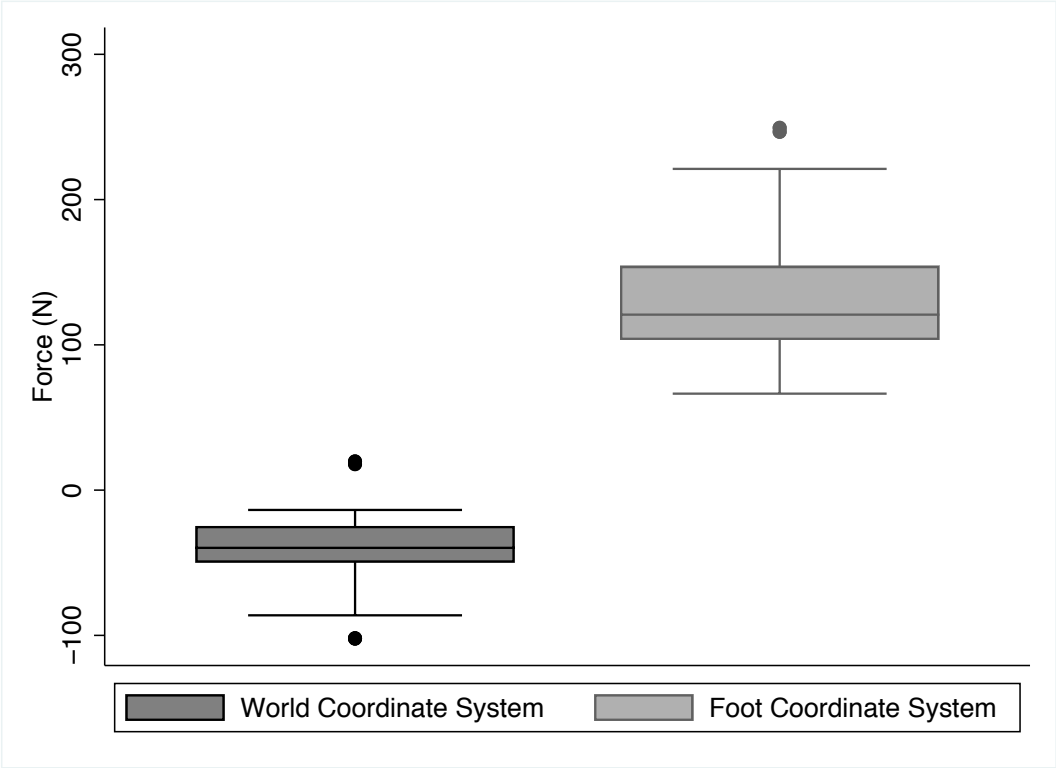

Figure 7: Maximum mediolateral (Y) forces for early braking (A) and late (B) phase of the stance.

A)

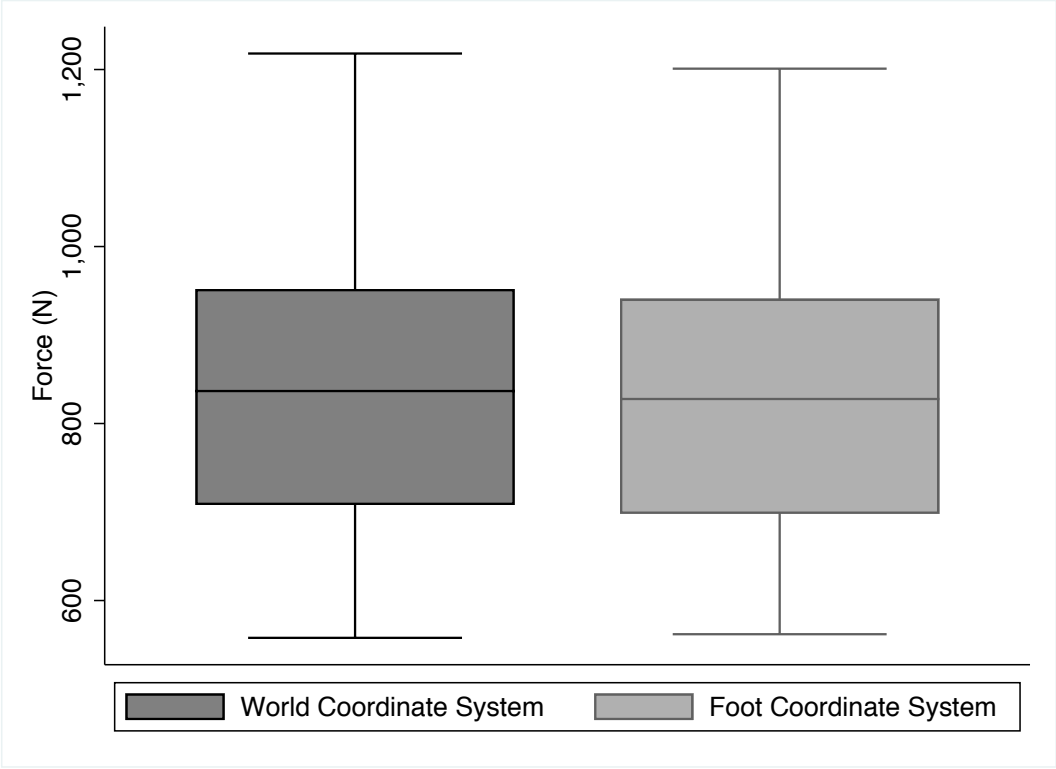

B)

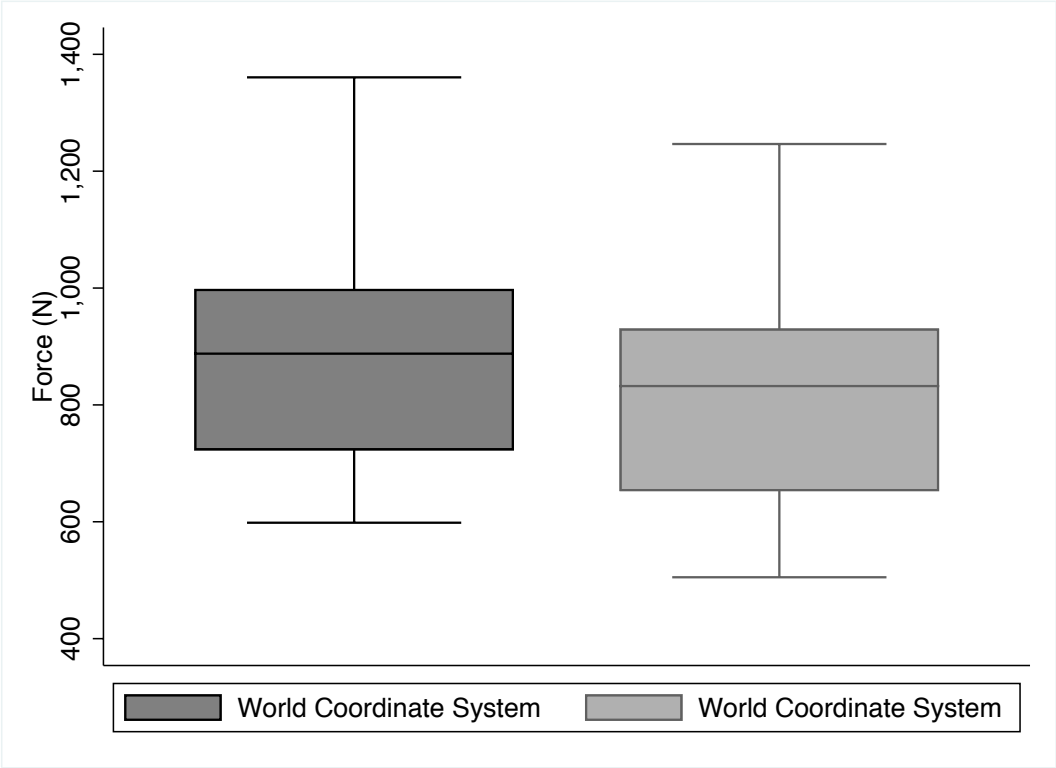

Figure 8: Maximum superioinferior (Z) forces for early braking (A) and late (B) phase of the stance.

Chapter 6: Conclusion and Future Work

In this final chapter, I will show how my results relate to the hypotheses laid out in my introduction, discuss how this work can be used to better interpret the hominin fossil record, and describe future work.

Hypotheses

Palpable landmarks on the external surface of the foot, like those used in gait studies, can be used to estimate the in vivo location of the talus.

My results indicate that the *in vivo* location of the can be predicted reliably from the location of external markers commonly used in gait studies. The navicular tubercle and both (lateral and medial) malleoli explained more of the variation of the center of the talar head (r^2 0.66-0.92; SEE: 1.7-2.3mm) and the medial (r^2 0.56-0.82; SEE: 2.2-3.2mm) and lateral (r^2 0.76-0.85; SEE: 1.0-1.9mm) points of posterior subtalar. Due to their close proximity to the talus, it is unsurprisingly that these three bony landmarks were predictive of the location of the joints. Nonetheless, the degree to which variation in internal position of the joints was predicted by external landmarks is encouraging for future FEA of the talus.

Walking while changing direction produces higher side forces that are applied to the human foot than when walking in a straight path.

Changing direction while walking does produce higher side forces that are applied to the human foot. I was able to illustrate the GRF components required to make a turn differ from those required to move in a straight path in both braking and propulsive phases of stance. During braking, the magnitude of both forward ($p<0.001$) and side forces ($p<0.001$) are higher in a turn

than for walking in a straight path. As an individual turns, the body slows in its current course in order to initiate the directional change, which requires a force at an angle to the initial direction of travel and in the new direction of travel. Similarly, the propulsive phase also shows an increase in the magnitude of forward forces ($p<0.001$) of on average 230N, an increase of 150%. Importantly, not only are the magnitudes of the GRF components higher ($p<0.001$), but the side force is on average 207 N higher (an increase of 2491%).

The manner in which forces pass through the foot is influenced by the foot's orientation.

In both early and late stance, maximum mediolateral forces are greater in the FCS than WCS. The increase in side forces in the FCS averages between 150-200 N, with some individuals exhibiting increases of greater than 350 N. The direction of the force also changes. In WCS the maximum force is directed toward the centerline, while in FCS it is lateral. Since the GRF magnitude does not change, this increase in side forces is due to decreases in the other two components. In both early stance, Z forces are relatively unchanged but in late stance FZ is somewhat less than WZ. Maximum WX is higher in magnitude than FX in early stance but not in late stance.

Implications for Paleo-Biomechanics

As the fossil evidence mounts, functional analysis of the modern foot and virtual simulation of variants of it become imperative. Although differences in foot shape in extinct forms imply the potential for differences in the kinetics of walking, understanding these differences requires biomechanical modeling.

Finite element analysis (FEA) offers a non-invasive solution that can be used to evaluate a variable of interest, like stress and strain (Rayfield, 2007), across many configurations. FEA is a powerful and flexible tool used by engineers to evaluate the static and dynamic behaviors of complex systems. Advances in computing power and software capabilities have made FEA more accessible to fields outside engineering, such as biology (Jongerius & Lentink, 2010), anthropology (Püschel & Sellers, 2016) and paleontology (Rayfield et al., 2001). These insights can then be used to make predictions about the function, especially in complex structures like the foot.

The foot and ankle have been the subjects of several FEMs. The majority of these studies focus on understanding force distribution through the foot in order to investigate injury mechanics and assist in developing medical countermeasures. Shin & Untaroiu (2012) developed a FEM of the foot and calf to understand the ankle and subtalar injuries associated with vehicle collisions. Spirka et al. (2014) created a simple FEM of the metatarsal heads to determine plantar pressure in the metatarsal head region in order to better design foot orthoses. Telfer et al. (2016) also modeled the metatarsal heads to investigate the utility of a simple FEM comparing to a more geometrically complex model, demonstrating that a simple model can provide plantar pressure predictions similar to a more complex model. These studies are often limited to understanding forces in a static position. In response to this, Qianet al. (2013) developed a FEM to apply dynamic loading conditions derived from gait measurements, covering the entire stance cycle. This study was limited, however, as the model is confined to the sagittal plane and the foot is represented by a simplified structure.

Morphological interpretations of fossils can be problematic without biomechanical interpretation. As discussed below, it is my hope that the findings presented in this dissertation

will be used to better understand the various fossils that are unearthed by increasing our understanding the biomechanics of the foot and ankle.

Conclusion

With this dissertation, I sought to better understand how forces impact the morphology of the human foot to advance our comprehension of the evolution of the hominin foot by investigating the forces that impact foot morphology. Not only does changing direction affect the ground reaction force applied to the foot, the orientation in which the foot is placed affects how these forces pass through the foot. Finally, this dissertation illustrated how external landmarks can be used to locate the talus, a bone that cannot be palpated but who's location is critical in order to fully understand the biomechanics of the foot an ankle.

In the end, this dissertation illustrated that our understanding of how the foot interacts with the ground is more complex than we typically thought as a result of the common phenomenon of changing direction.

Future Work

I plan on continuing to explore the biomechanics of the foot and ankle, and the data that I collected for this dissertation will allow me to explore many additional research avenues. The three chapters above only skimmed the surface of what this dataset could achieve in order to further our understanding of the evolution of the hominin foot. Some, though not all that could be imagined, of the future work that I intend to do using this dataset is presented below.

Prediction of additional joints in the foot – The dataset that was used for chapter 3 of this dissertation has the potential of creating regression-based equations for additional joints within the foot, such as the calcaneal-cuboid joint. Like the two joints explored in chapter 3, all of these

joints are buried deep within the foot but important to understand how forces transfer from bone to bone.

Investigating the foot kinematics of turning – This dissertation's primary focus was on the kinetic differences that are seen due to changing direction. How the body physically responds to a turn is the next logical step using this dataset. The 3D trajectories from these trials could be analyzed in order to see how the body is physically making adjustments in order to make these directional changes, both before and after a turn occurs.

Anticipation of turning – In Chapter 4, this dissertation only used forces that were generated from two of the three force plates. By looking at the step that occurs between the first and third force plate I hope to better understand what the opposite leg is doing when the body is preparing to make a directional change.

Turning in multiple directions – The structure of the larger protocol that was established for this dissertation was regimented such that turning condition was controlled, meaning that all individual's turn was in the same direction. Data collection, however, included trials where individuals walked in the opposite direction in order to collect force and motion data for turns in the opposite direction. It is my hope to take these trials and compare them to see if there is a kinetic and kinematic difference simply from turning in the opposite direction.

Different turning patterns – The dataset from this dissertation also included two additional turning conditions: a 45° turn (turning direction is contralateral to the stance foot) and a 45° turn where the swing foot crosses over the stance foot in order to change direction (turning direction is ipsilateral to the stance foot).

Joint moments – This dissertation only investigated a small aspect of the overall biomechanics of the foot, specifically the ground reaction forces. How the joints of the ankle,

like the talonavicular and posterior subtalar joints, respond to these forces is a logical next step in my research trajectory.

Foot deformation while walking – While not specific to directional changes, the 3D marker set used for this dissertation included a trajectory that was placed where the calcaneus and the foot's fat pad meet. This marker could be investigated along with the other markers of the foot in order to understand how the soft tissues of the foot respond to the high impacts of striking the ground while walking.

How the rest of the body responds to turning - The protocol created for this dissertation also included markers on the thigh, hips, torso, and arms. While these areas are not traditionally thought of when researching foot biomechanics, the joints connecting these areas are influenced by changes in applied force. The kinetic and kinematic data from this dissertation can be used to investigate how other regions of the body respond to the forces associated with directional changes.

Creation and validation of a Finite Element Model of the talus – My ultimate plan for the dissertation data is to use the forces collected for this dissertation in order a validated finite element model (FEM), which will connect form and function in the modern human talus. It is my hope that an FEM can be used to not only understand how the talus responds to the applied forces to the body but that this FEM could also be morphed in order to represent morphological forms of our hominin ancestors.

Chapter 6: Appendix

Chapter 6: References

Jongerius, S. R., & Lentink, D. (2010). Structural Analysis of a Dragonfly Wing. *Experimental Mechanics*, *50*(9), 1323–1334. https://doi.org/10.1007/s11340-010-9411-x

Püschel, T. A., & Sellers, W. I. (2016). Standing on the shoulders of apes: Analyzing the form and function of the hominoid scapula using geometric morphometrics and finite element analysis. *American Journal of Physical Anthropology*, *159*(2), 325–341. https://doi.org/10.1002/ajpa.22882

Qian, Z., Ren, L., Ding, Y., Hutchinson, J. R., & Ren, L. (2013). A Dynamic Finite Element Analysis of Human Foot Complex in the Sagittal Plane during Level Walking. *PLoS ONE*, *8*(11), e79424. https://doi.org/10.1371/journal.pone.0079424

Rayfield, E. J. (2007). Finite Element Analysis and Understanding the Biomechanics and Evolution of Living and Fossil Organisms. *Annual Review of Earth and Planetary Sciences*, *35*(1), 541–576. https://doi.org/10.1146/annurev.earth.35.031306.140104

Rayfield, E. J., Norman, D. B., Horner, C. C., Horner, J. R., Smith, P. M., Thomason, J. J., & Upchurch, P. (2001). Cranial design and function in a large theropod dinosaur. *Nature*, *409*(6823), 1033–1037. https://doi.org/10.1038/35059070

Shin, J., Yue, N., & Untaroiu, C. D. (2012). A Finite Element Model of the Foot and Ankle for Automotive Impact Applications. *Annals of Biomedical Engineering*, *40*(12), 2519–2531. https://doi.org/10.1007/s10439-012-0607-3

Spirka, T. A., Erdemir, A., Ewers Spaulding, S., Yamane, A., Telfer, S., & Cavanagh, P. R. (2014). Simple finite element models for use in the design of therapeutic footwear. *Journal of Biomechanics*, *47*(12), 2948–2955. https://doi.org/10.1016/j.jbiomech.2014.07.020

Telfer, S., Erdemir, A., Woodburn, J., & Cavanagh, P. R. (2016). Simplified versus geometrically accurate models of forefoot anatomy to predict plantar pressures: A finite element study. *Journal of Biomechanics*, *49*(2), 289–294. https://doi.org/10.1016/j.jbiomech.2015.12.001